

# Sorption-Enhanced Dry Reforming of Methane in a DBD Plasma Reactor for Single-Stage Carbon Capture and Utilization

Rani Vertongen, Giulia De Felice, Huub van den Bogaard, Fausto Gallucci, Annemie Bogaerts, and Sirui Li\*




Cite This: *ACS Sustainable Chem. Eng.* 2024, 12, 10841–10853



Read Online

ACCESS |

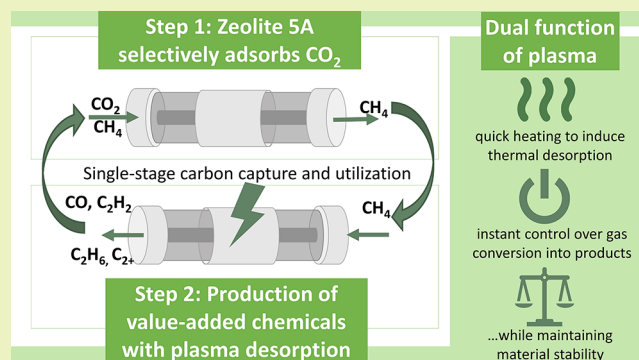
 Metrics & More

 Article Recommendations

 Supporting Information

**ABSTRACT:** Plasma–sorbent systems are a novel technology for single-stage carbon capture and utilization (CCU), where the plasma enables the desorption of CO<sub>2</sub> from a sorbent and the simultaneous conversion to CO. In this study, we test the flexibility of a plasma–sorbent system in a single unit, specifically for sorption-enhanced dry reforming of methane (DRM). The experimental results indicate the selective adsorption of CO<sub>2</sub> by the sorbent zeolite 5A in the first step, and CH<sub>4</sub> addition during the plasma-based desorption of CO<sub>2</sub> enables DRM to various value-added products in the second step, such as H<sub>2</sub>, CO, hydrocarbons, and the byproduct H<sub>2</sub>O. Furthermore, our work also demonstrates that zeolite has the potential to increase the conversion of CO<sub>2</sub> and CH<sub>4</sub>, attributed to its capability to capture H<sub>2</sub>O. Aside from the notable carbon deposition, material analysis shows that the zeolite remains relatively stable under plasma exposure.

**KEYWORDS:** plasma, dry reforming of methane, dielectric barrier discharge, sorbent, carbon capture and utilization, zeolite



shows that the zeolite remains relatively stable under plasma

## HIGHLIGHTS

- Value-added products formed by adsorption of CO<sub>2</sub> and desorption in a CH<sub>4</sub> plasma.
- Plasma heating contributes to the thermal desorption of CO<sub>2</sub>.
- Zeolite 5A is beneficial to DRM because it captures the byproduct H<sub>2</sub>O.
- No significant plasma-induced changes in surface area and morphology of sorbents.

## 1. INTRODUCTION

Global warming is a complex problem, and there is significant pressure for urgent action and meaningful change.<sup>1</sup> In the transition to a more sustainable society, defossilization is crucial to reducing CO<sub>2</sub> emissions in the chemical industry through electrification and carbon capture, utilization, and storage.<sup>2,3</sup> Although carbon capture and storage (CCS) is most promising to decrease CO<sub>2</sub> emissions effectively in the short term,<sup>4,5</sup> large-scale projects are only just starting.<sup>6</sup> Known limitations are the high cost of separation, enrichment, transportation of CO<sub>2</sub>, and the negative impact on ecology associated with physical storage.<sup>7,8</sup> Alternatively, carbon capture and utilization (CCU) aims to apply the captured CO<sub>2</sub> into products or convert it into value-added chemicals and fuels through electrified technologies.<sup>9</sup> Not only does this

decrease our dependence on fossil fuels, but also it can help to store the excess and uncertain supply of renewable electricity as stable chemical energy.<sup>10</sup> However, many CCU processes still require multiple stages from the adsorption to the utilization, and possible steps in between stages, such as the transport and storage of CO<sub>2</sub>.<sup>11</sup>

One way to circumvent these steps is to apply single-stage CCU and reduce the overall process cost.<sup>12</sup> More specifically, “single-stage” CCU refers to the integrated capture and utilization of CO<sub>2</sub> in one process, particularly within a single reactor unit. For example, with adsorption-based carbon capture, CO<sub>2</sub> is first captured from a dilute source such as flue gas (~15 vol % CO<sub>2</sub>) or direct air capture (DAC).<sup>13</sup> Then, the adsorbed CO<sub>2</sub> is converted *in situ* while simultaneously regenerating the sorbent. The concept falls within the domain of “integrated carbon capture and utilization (ICCU)”, which has been described by Liu et al.,<sup>14</sup> despite the potential ambiguity associated with the term “integrated” within the context of process design.

**Received:** March 25, 2024

**Revised:** June 27, 2024

**Accepted:** June 28, 2024

**Published:** July 6, 2024



Various technologies have already been proposed when considering solely the conversion of CO<sub>2</sub>. The thermocatalytic approach typically applies a reducing atmosphere such as H<sub>2</sub> or CH<sub>4</sub> to enable generally high-temperature conversion with various catalysts.<sup>12</sup> Alternative technologies are also gaining increasing attention, such as electro-,<sup>15</sup> photo-,<sup>16</sup> and plasma-catalytic<sup>17</sup> conversion steps, thanks to their operation at ambient pressure and temperature. Plasma technology is a particularly flexible solution for CO<sub>2</sub> conversion since it can be easily switched on/off with immediate production, and it does not rely on rare metal catalysts for good performance.<sup>18</sup> The energetic electrons and reactive species in the plasma can activate stable molecules at ambient conditions, resulting in a wide range of gas conversion applications, as summarized by Bogaerts et al.<sup>19</sup>

However, in realistic applications, scenarios often involve the presence of contaminants or, conversely, low CO<sub>2</sub> concentrations, necessitating enrichment through processes involving adsorbents, as seen in DAC. Several reported studies have focused on addressing these challenges, including not only the effect of impurities<sup>20</sup> but also the combination with sorbents in plasma-based CCU in a one-stage<sup>17,21–25</sup> and double-stage configuration.<sup>26–30</sup> Yoshida et al.<sup>21</sup> studied the desorption of CO<sub>2</sub> when the sorbent material is placed inside the plasma zone. They even demonstrated faster desorption with plasma than with a thermal approach, and they attributed this effect to the interaction of the electrons and reactive species in the plasma with the sorbent material. Li et al.<sup>22</sup> proposed CO<sub>2</sub> capture with a hydrotalcite sorbent and plasma-based desorption and conversion in a dielectric barrier discharge (DBD) plasma reactor. By further optimizing the experimental conditions, they achieved a maximum single-pass conversion of 60%.<sup>17</sup> They also tested the periodic operation of multiple reactors in parallel and in series for continuous operation, which resulted in the full conversion of CO<sub>2</sub> into CO and O<sub>2</sub> in the outlet stream.

Furthermore, the potential of plasma-based single-stage CCU can be extended beyond the splitting of CO<sub>2</sub> for CO production, also to the production of value-added chemicals through CO<sub>2</sub> hydrogenation or dry reforming of methane (DRM). Kaikkonen<sup>23</sup> tested dual-functional materials for the reaction of adsorbed CO<sub>2</sub> with H<sub>2</sub> and found that the organic Hydrocell-resin had the highest adsorption capacity and a CO<sub>2</sub> conversion of 15%. Despite this, there have been limited studies reported in this field thus far, particularly regarding DRM, which could be more complex due to its involvement in the capture and conversion of both CO<sub>2</sub> and CH<sub>4</sub>. Gorky et al.<sup>24</sup> investigated plasma-based desorption of CH<sub>4</sub> and CO<sub>2</sub> using MOF-177 as the sorbent. Notably, the gases were not mixed during the process in their study. In a subsequent study, various silicoaluminophosphate (SAPO) zeolites were employed, revealing that higher acidity or larger pore size contributes to a slower desorption rate.<sup>25</sup> Nevertheless, for DRM in a plasma–sorbent system, many important aspects require more investigation, including the impact of plasma on the sorbent, desorption mechanisms, and potential reactions between CO<sub>2</sub> and CH<sub>4</sub>.

To the best of our knowledge, no previous research has investigated DRM with a plasma–sorbent system for single-stage CCU. Despite the significant potential of this topic, the novel concept requires validation and a deeper understanding of the interaction between plasma and sorbents. Such studies would also benefit practical applications, particularly in

improving the coupling of gas mixtures such as biogas<sup>31</sup> and landfill gas<sup>32</sup> to the plasma through the utilization of sorbents. Hence, this study focuses on experimentally investigating sorption-enhanced DRM using a plasma–sorbent system. Solid sorbents are combined with nonthermal plasma within a single DBD reactor. The research delves into plasma-induced desorption and conversion of CO<sub>2</sub> and CH<sub>4</sub> to demonstrate the single-stage CCU for DRM, with a discussion on possible underlying mechanisms.

## 2. METHODS

**2.1. Experimental Setup.** The experimental setup including the DBD reactor used in this study is shown in Figure 1; more details can

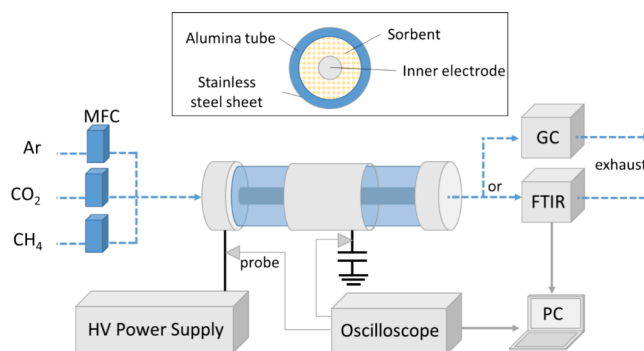


**Figure 1.** Experimental setup for plasma-induced CO<sub>2</sub> desorption and conversion.

be found in our previous publication.<sup>17</sup> The dielectric barrier of the reactor was an alumina tube with external and internal diameters of 12.9 mm and 8.6 mm, respectively. A thin stainless-steel sheet (100 mm long) was placed around the tube and connected to the ground via a 100 nF capacitor. The inner electrode was a stainless-steel rod with a diameter of 6.7 mm, resulting in a discharge gap of 0.95 mm. The electrode was connected to the AC high-voltage power supply (AFS G155–150 K) fixed at 45 kHz. A four-channel oscilloscope (PicoScope 3405D, 100 MHz, 8-bit sampling rate of 1 G/s) was used to record the voltage waveforms. A 1:1000 high-voltage probe (Tektronix P6015A) was used to monitor the voltage (V) across the reactor. To measure the charge (Q) transferred during the plasma discharge, a 1:10 probe (Pico TA 131) measured the voltage across a 100 nF capacitor. To calculate the discharge power, both waveforms were recorded to form Lissajous figures.<sup>33</sup>

The inlet flow rate was controlled by mass flow controllers (Bronkhorst, calibrated at 0 °C and 1.013 bar) for Ar, CO<sub>2</sub>, and CH<sub>4</sub>. After the reactor, the outlet gas flowed to a Fourier transform infrared spectroscopy (FTIR) spectrometer (Agilent Technology, Cary 630) to analyze the gas composition as a function of time. The spectrometer has a gas cell with CaF<sub>2</sub> windows, connected to a RED-SHIFT gas sampling system, and a scan resolution of 4 cm<sup>-1</sup>. All measurements were performed at room temperature (no external temperature control supplied to the reactor) and atmospheric pressure. The FTIR spectra were collected, and the concentrations of the components were calculated with the software Kinetic Pro and Microlab. An additional measurement was performed by connecting the outlet gas to an in-line gas chromatograph (GC, Thermo Scientific Trace 1300) equipped with two thermal conductivity detectors and a flame ionization detector. A small N<sub>2</sub> flow (5 mL<sub>n</sub>/min) was added after the plasma reactor as an internal standard. This allowed the identification of C<sub>1</sub>–C<sub>3</sub> hydrocarbons that overlap with the CH<sub>4</sub> peaks in the FTIR spectrum and IR-inactive molecules such as H<sub>2</sub>. It is important to note that GC measurements require a longer duration for sampling and analysis (approximately 15 min per measurement in our case). This prohibits continuous measurements during the desorption stage, with short intervals between samples to capture the

transient behavior of gas composition, as achievable with FTIR (10 s per measurement). Hence, we conducted GC measurements through a series of repeated experiments, where each measurement is taken at specific times after plasma ignition. To study the influence of water, a simple humidity meter (Extech Instruments Humidity Alert II 445815) was installed in the exhaust line. The relative humidity is measured, i.e., the actual amount of water vapor in the air compared to the total amount of vapor that can exist in the air at the current temperature.<sup>34</sup> To study the outside reactor temperature, a small thermal camera (FLIR ONE Pro) was installed on the USB-c port of an Android smartphone. It was installed on a stand such that the camera could capture the warm region of the reactor.

We used 2.3 g of zeolite 5A beads (LTA type zeolite, mesh 8–12, Sigma-Aldrich) in this study, modified to a size of 250–355  $\mu\text{m}$ . Pretreatment in plasma was performed to remove any ambient  $\text{H}_2\text{O}$  and  $\text{CO}_2$  that might be adsorbed on the material (see Section 2.2 for an exact description of the conditions). This commercial molecular sieve is also commonly applied in industry and investigated for adsorption.<sup>35,36</sup> In principle, it is possible to use other sorbents that have been reported in the literature.<sup>37–39</sup> For example, Li and Gallucci<sup>17</sup> previously used hydrotalcite pellets. Despite their good performance, this material requires more extensive pretreatment (up to 6000 s of plasma exposure) to remove the  $\text{H}_2\text{O}$  that is inherently present in the structure. Furthermore, these pellets are relatively brittle compared to other commercial sorbents. We conducted pretests on zeolite 4A, the results of which are presented in the Supporting Information (SI), Section S1, revealing a low  $\text{CO}_2$  capacity. Therefore, we opted for zeolite 5A owing to its good stability and higher  $\text{CO}_2$  capacity. This test highlights the importance of sorbent choice, compared to the field of plasma catalysis, where adsorption and desorption have not been investigated thoroughly in typical studies. In addition, quartz particles within the same size range were packed and tested under the same experimental conditions. This control measurement served as a reference to quantify any delays in the measurement due to the volume of the lines and the stabilization time of the mass flow controllers.

To study the effect of plasma exposure, the material was characterized before and after plasma treatment. The morphology of the surface was investigated through scanning electron microscopy (SEM) with a Phenom Microscope ProX equipped with a backscattered electron detector (BSD) and a secondary electron detector (SED). The images were collected at several magnifications. Furthermore, the surface area and the pore volume were investigated through nitrogen physisorption at  $-196\text{ }^\circ\text{C}$  with a TriStar 3000 Micromeritics, applying the Brunauer–Emmett–Teller (BET) plot method and the Barret–Joyner–Halenda (BJH) method.

**2.2. Adsorption–Desorption Procedure.** The general procedure is summarized in Table 1. All experiments were performed at atmospheric pressure, and no external heating or cooling was applied to the reactor, besides the influence of the plasma. Three repeated experiments were performed for each sorbent with the same sorbent sample; the small effect of the separate runs on the adsorption is displayed in the SI, Section S2.

**Table 1. Overview of the General Adsorption–Desorption Procedure in the DBD Plasma Reactor at Atmospheric Pressure and Room Temperature (No External Temperature Control)**

	time (s)	Ar ( $\text{mL}_n/\text{min}$ )	$\text{CO}_2$ and/or $\text{CH}_4$ ( $\text{mL}_n/\text{min}$ )	plasma power (W)
pretreatment	1800	40	0	30
cooldown	1800	100	0	0
adsorption	800	20	20	0
flushing	1000	100	0	0
desorption	800	40	0	30
cooldown	1800	100	0	0

Fresh sorbent material was pretreated with plasma to remove any ambient  $\text{H}_2\text{O}$  or  $\text{CO}_2$  from the surface. In the adsorption stage, a mixture of the adsorption components was fed to the reactor until the sorbent material was saturated. To clear the lines and remove any nonadsorbed  $\text{CO}_2$  and  $\text{CH}_4$ , the reactor was flushed with a high flow of Ar. This also ensures that we only measured surface desorption and conversion in the desorption step. Finally, in the desorption step, the plasma was switched on to induce desorption. We applied a frequency of 45 kHz and a constant plasma power of ca. 30 W. More details on the plasma power are presented in the SI, Section S3. After each plasma treatment, the reactor was flushed with Ar for 1800 s to cool down to below  $40\text{ }^\circ\text{C}$  (measured with a thermal camera on the reactor). Since the adsorption capacity of zeolites decreases due to plasma heating, this approach was needed to maintain consistency in the amount of  $\text{CO}_2$  adsorbed in all tests.

For calculating the adsorbed and desorbed volumes, the total volumetric flow rate is based on the flow rate of Ar, which is set at a constant input value and assumed to be inert, and the molar concentration of Ar. The component-specific flow rate is determined by multiplying the total flow rate with the molar fraction of interest. The total amount of adsorbed and desorbed components was calculated from the integration of the differential concentration over time and corrected for the blank measurement. For the total volume, the integration was made over the entire desorption period (50–450 s), while for the instantaneous volume, the integration was made over the period between two measurements, which is 10 s. These values were averaged over the three repeated experiments to determine the experimental error. While TGA is the conventional method to determine the  $\text{CO}_2$  capacity in material science, we want to stay consistent with the plasma tests, to improve our understanding of the plasma process. Since the adsorption capacity can be influenced by plasma exposure, the capacity calculated via the plasma tests is more reliable, especially since we calculate the average value over three runs.

We can estimate  $\text{CO}_2$  conversion based on the production of CO, similar to previous work on plasma-based  $\text{CO}_2$  splitting<sup>17,40</sup>:

$$\begin{aligned} \text{estimated conversion}[\%] &= \frac{\text{CO produced}}{\text{total desorption}(\text{CO} + \text{CO}_2)} \times 100[\%] \end{aligned} \quad (1)$$

It should be noted that the estimated conversion in this case is not the actual representation of the conversion, but a rough estimation to evaluate the chemical process. In some experiments,  $\text{CH}_4$  also plays a role in the plasma and value-added products can be formed. Furthermore, significant carbon deposition on the packing and some condensation at the outlet were observed, making it unfeasible to complete the carbon and hydrogen balance. For example, the measured CO may be formed not only from  $\text{CO}_2$  conversion but also possibly from the oxidation of carbon at the surface.<sup>41</sup> In addition, the measured concentrations are time-dependent in this nonsteady-state process, which means that the typical calculations and correction for the gas expansion, such as those described by Wanten et al.<sup>40</sup> for flow plasma reactors, are invalid in our case. This is especially difficult for calculations regarding energy efficiency and cost: due to the significant desorption in these experiments, the variable flow rate is not suitable to determine the specific energy input. Alternatively, we calculate the energy yield based on the duration of the desorption peak and the production of CO:

$$\begin{aligned} \text{estimated energy yield}[\text{mmol}\cdot\text{kJ}^{-1}] &= \frac{\text{CO produced}[\text{mmol}]}{\text{plasma power}[\text{kW}] \times \text{desorption interval}[\text{s}]} \end{aligned} \quad (2)$$

The purpose of using Ar during the desorption stage is to use it as a carrier gas to create a flow that enables the measurement of transient concentrations, to study the time-dependent behavior of the plasma-sorbent system. For practical application, a different low-cost carrier gas would be more interesting. It should be noted that switching the discharge gas will alter the plasma properties and a detailed investigation of the effect on the desorption procedure would be

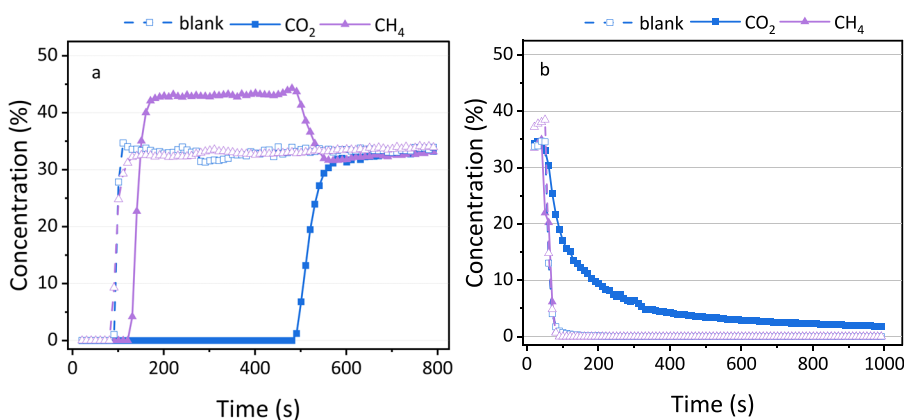


**Figure 2.** Concentration of CO<sub>2</sub> and CH<sub>4</sub> in the outlet stream (a) during the adsorption stage and (b) during the flushing stage. The solid points are for the zeolite, while the open symbols are for the blank measurements with quartz.

needed. A discussion on a more realistic process is given in the Outlook, Section 4.

### 3. RESULTS AND DISCUSSION

**3.1. Operation with CO<sub>2</sub>/CH<sub>4</sub> Feed Gas.** In our first set of experiments, we applied a 1/1/1 CO<sub>2</sub>/CH<sub>4</sub>/Ar mixture as the feed gas in the plasma–sorbent system, with Ar as the internal standard. The experiment was performed according to the general outline described in Table 1 and is presented in more detail in the SI, Section S4. Notably, the pretreatment and cooldown steps remain consistent across all experiments and are thus not explicitly described here but presented in the SI, Section S5.

**3.1.1. Adsorption and Flushing.** Figure 2a displays an example of concentration measured as a function of time for each component during the adsorption step. The open symbols represent the blank measurement over quartz sand, which reveals a measurement delay of approximately 100 s. Since this material does not adsorb either CO<sub>2</sub> or CH<sub>4</sub>, this delay primarily arises from the time required for the gas to travel through the pipeline and reach the gas cell of the FTIR for measurement.

The blank material has a simultaneous breakthrough of CO<sub>2</sub> and CH<sub>4</sub> reaching about 33%, as expected since no gas is adsorbed, and the feed gas has a 1/1/1 CO<sub>2</sub>/CH<sub>4</sub>/Ar ratio. In contrast, for sorbent material zeolite 5A, we observe a clear difference between CO<sub>2</sub> and CH<sub>4</sub>. The breakthrough of CH<sub>4</sub> is very fast, and only slightly later than for quartz sand, indicating that no significant amount of CH<sub>4</sub> adsorbs on zeolite 5A. This is also confirmed by the results obtained in the flushing and desorption steps, as described in the following sections. The small delay in the CH<sub>4</sub> concentration compared to the blank can be attributed to the reduced total flow rate due to CO<sub>2</sub> adsorption, which slightly increases the residence time in the gas lines between the reactor and the FTIR. Likewise, the higher concentration (about 45%) compared to the blank is also attributed to CO<sub>2</sub> adsorption, as there is now relatively more CH<sub>4</sub> in the mixture. For CO<sub>2</sub>, the breakthrough occurs at a much later time, indicating significant adsorption until the material is saturated after 500 s. Based on three repeated experiments, we calculate an adsorbed volume of 126 ± 1 mL, corresponding to an adsorption capacity of 2.4 mmol/g in line with the literature on zeolite 5A.<sup>42</sup> After the sorbent is saturated, CO<sub>2</sub> remains in the gas stream, explaining the rise in its concentration and leading to a decrease in the relative

concentration of CH<sub>4</sub> to a value of about 33%, similar to the blank experiment.

The difference between CO<sub>2</sub> and CH<sub>4</sub> in Figure 2a demonstrates a preferential interaction of zeolite 5A with CO<sub>2</sub> instead of CH<sub>4</sub>, as proven in specific literature on zeolite 5A<sup>42</sup> and similar materials.<sup>43,44</sup> For gas mixtures such as biogas, CO<sub>2</sub> can selectively adsorb on zeolite 5A to give a purer CH<sub>4</sub> outlet stream. This can be explained by the material properties and the polarizability of the molecules. The quadrupole moment of CO<sub>2</sub> can induce electrostatic interactions with the cations in the zeolite (Ca<sup>2+</sup> and Na<sup>+</sup>).<sup>45</sup> CH<sub>4</sub> has no quadrupole moment,<sup>45</sup> and only weaker induction interactions are possible with the zeolite due to the polarizability of the molecule. Some materials might be more suitable for CH<sub>4</sub> capture,<sup>46,47</sup> but the competition with CO<sub>2</sub> is usually not accounted for. In our study, we selected zeolite 5A due to its suitability for the outlined objectives (Section 2.1), and we focused on establishing the proof of concept for sorption-enhanced DRM. Further screening and optimization of sorbent materials is recommended for future study.

Note that the CO<sub>2</sub> and CH<sub>4</sub> concentrations and flow rates chosen for this study are based on experimental constraints and the capabilities of the setup. In real-world scenarios, concentrations vary widely depending on the source, from high levels in biogas<sup>31</sup> and landfill gas<sup>32</sup> to very low concentrations in flue gas or air. Additionally, zeolite sorbents, like the one in this study, are also investigated for DAC.<sup>48</sup> Given that only CO<sub>2</sub> is adsorbed, the CO<sub>2</sub>/CH<sub>4</sub> ratio is less influential as it only affects the adsorption duration. Thus, the conditions selected for this study were chosen to ensure a reasonable duration for experimentation.

The flushing step removes any residual gas to ensure that the following desorption step is a true representation of only the adsorbed molecules. Figure 2b illustrates the concentration of CO<sub>2</sub> and CH<sub>4</sub> during flushing as a function of time. In the blank experiments, after the initial delay due to the gas lines, the concentration drops immediately for both gas components. The same behavior is observed for the concentration of CH<sub>4</sub> in the case of zeolite 5A. The reduction in CO<sub>2</sub> concentration occurs slowly, suggesting a gradual release of CO<sub>2</sub> from the sorbent. The flushed volume of CO<sub>2</sub> is calculated as 53 ± 2 mL, which is about 40% of the total adsorbed volume. Due to its quadrupole moment, CO<sub>2</sub> will mostly interact through physisorption with the zeolite, as previously explained. This interaction is notably weaker compared to chemisorption or

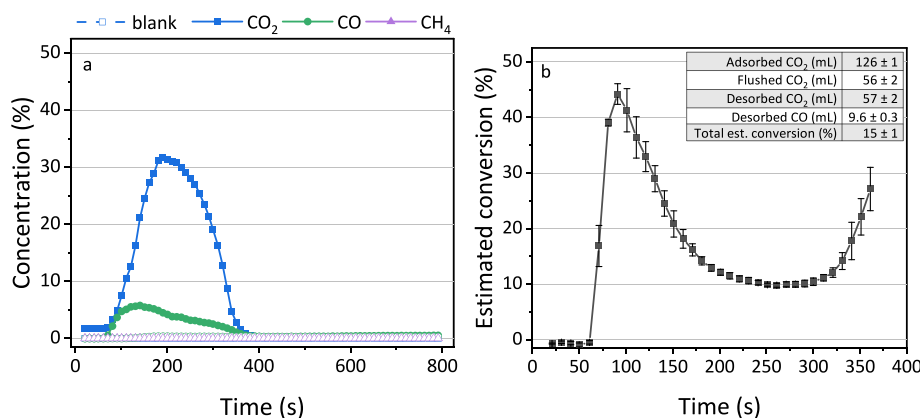


**Figure 3.** (a) Concentration of CO<sub>2</sub>, CO, and CH<sub>4</sub> in the outlet stream during the plasma treatment. The solid points are for the zeolite, while the open symbols are for the blank measurements with quartz. (b) Estimated conversion at every time interval during CO<sub>2</sub> desorption. The values after 360 s are not accurate because the areas are too small; the estimated conversion will drop to zero in reality. The inset summarizes the volumes and total conversion.

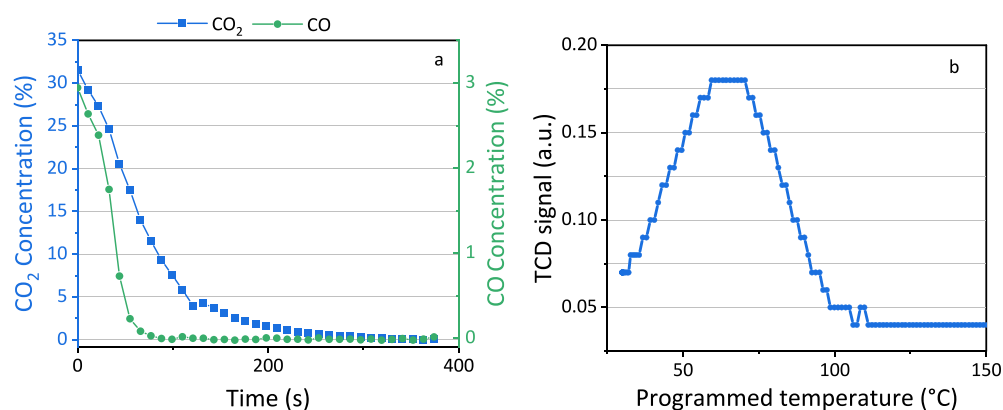


**Figure 4.** (a) Concentration of CO<sub>2</sub> and CO (left and right y-axis, respectively) as a function of time after the plasma is turned off (treatment time of 200 s of plasma desorption). (b) Temperature-programmed desorption (TPD) of zeolite 5A with the thermal conductivity detector (TCD) signal in arbitrary units, representing the CO<sub>2</sub> desorption. The step size of the y-axis was set to 0.01, explaining the step-like profile of the curve.

stronger dipole interactions. The gradual decline depicted in Figure 2b indicates that a significant amount of weakly adsorbed CO<sub>2</sub> is flushed away from the material, alongside the gas trapped between the pellets. For this proof of concept in this work, this relatively long flushing step was chosen to eliminate the influence of gas residue in the reactor and pipeline, in order to determine the real desorption induced by plasma in the next step. For realistic applications, it is crucial to design shorter flushing steps while also ensuring that weakly adsorbed CO<sub>2</sub> can be effectively treated by plasma for conversion.

**3.1.2. Desorption and the Influence of Temperature.** The plasma is ignited in Ar with a power of ca. 30 W to induce desorption and conversion. Figure 3a displays the concentrations measured in the outlet stream as a function of time during the desorption.

CO<sub>2</sub> desorption from the material is evident, while no CH<sub>4</sub> desorption is detected, consistent with earlier observations of minimal CH<sub>4</sub> adsorption on the zeolite. While DRM requires both CO<sub>2</sub> and CH<sub>4</sub>, noticeable adsorption and subsequent desorption are observed exclusively for CO<sub>2</sub>. Nevertheless, CO was detected in the outlet gas stream, indicating that CO<sub>2</sub> splitting occurs during plasma exposure since typically only CO and O<sub>2</sub> are formed in DBD plasmas in CO<sub>2</sub>.<sup>49</sup> The mechanisms for CO<sub>2</sub> splitting during desorption were

discussed in a previous work by Li et al.,<sup>22</sup> where two routes were suggested: the adsorbed CO<sub>2</sub> can desorb and convert to CO in the gas phase, or the adsorbed CO<sub>2</sub> can be split directly and produce gas-phase CO. Even though a different sorbent material was tested in this work, the same mechanisms probably play a role here.

By integrating the area under the curve, we calculated a desorbed volume of 57 ± 2 mL for CO<sub>2</sub> and a volume of 9.6 ± 0.3 mL for CO. In addition to the flushed volume of 56 ± 2 mL in Figure 2b, we obtained a total volume of 120 ± 3 mL that was removed from the sorbent. This corresponds to 95% of the total adsorbed volume of CO<sub>2</sub> (126 ± 1 mL; Figure 2a). The 5% difference may be caused by the resolution of the FTIR. Although the measurements are taken every 10 s, it still could introduce an error on the steep gradients in our results. Despite this small deviation, we can determine the estimated conversion as 15 ± 1% according to eq 1, using the total areas of the CO<sub>2</sub> and CO peaks. The maximum estimated transient conversion, calculated for each point, is 44 ± 2% obtained around 91 s (see Figure 3b). The highest value is expected at the beginning of the desorption peak since CO<sub>2</sub> is heavily diluted in Ar. It is well known for CO<sub>2</sub> conversion in DBD plasma that dilution in Ar can improve the conversion.<sup>50</sup> Notably, a rise in CO<sub>2</sub> concentration correlates with a decreasing conversion, and vice versa, indicating a direct

inverse relationship between these two parameters. Still, both estimated conversions are in the range of typical values obtained in DBD plasmas.<sup>52</sup> The estimated energy yield is 0.047 mmol  $\text{kJ}^{-1}$  (see eq 2). A desorption time of 300 s was chosen because this was the time of most significant conversion. This is significantly lower than the energy yield obtained in  $\text{CO}_2$  conversion in flow DBD reactors. In the work by Wang et al.,<sup>51</sup> where a zeolite 5A packing similar to this work was used, they had a similar  $\text{CO}_2$  conversion 15% but a much better energy yield of 33.3 mmol  $\text{kJ}^{-1}$ . However, we cannot directly make this comparison with the energy efficiency and cost in steady-state flow reactors (as discussed in Section 2.2). It should be mentioned that the aim of this work was solely to demonstrate the proof of concept. Further optimization to improve performance can be achieved through enhanced sorbent capacity, better reactor design, and refined operation parameters, which will be investigated in the future.

To verify the desorption and reaction mechanism in our system with the zeolite sorbent, we ran the plasma-desorption step for 200 s and then we switched off the plasma during desorption and started the measurement. Figure 4a depicts the  $\text{CO}_2$  and CO concentrations as a function of time, starting when the plasma was switched off. The CO concentration drops abruptly, proving that there is no conversion without plasma. However, the  $\text{CO}_2$  concentration decreases more gradually when the plasma is switched off. Although  $\text{CO}_2$  has a higher initial concentration, which could influence the decrease rate, in our experimental system, the continuous Ar flush at 40  $\text{mL}_g/\text{min}$  could decrease the  $\text{CO}_2$  concentration to <1% within 100 s if no further desorption occurred. Instead, we observed a sustained  $\text{CO}_2$  concentration >1% until 220 s. This indicates that the desorption does not stop instantly, as in the case of CO. The sustained desorption is primarily attributed to the thermal effect, resulting from the plasma heating of the sorbent.

Temperature-programmed desorption (TPD) was conducted to study the thermal desorption profile, and the result is presented in Figure 4b.  $\text{CO}_2$  desorbs from zeolite 5A at temperatures between 40 and 100  $^\circ\text{C}$ . Even though DBD generates a relatively cold plasma, the temperature increase of the sorbent could easily reach the level needed for desorption on zeolite 5A.<sup>49,53</sup> Especially the localized plasma heating, which is widely acknowledged as the so-called “hot spots”,<sup>54</sup> could play an important role. Direct measurement of the sorbent surface temperature is not feasible in our case. Instead, we installed an IR camera to estimate the temperature of the reactor wall during plasma operation as an indication.

The results are presented in Figure 5, and an approximate comparison with TPD-MS is presented in the SI, Section S6. It is important to note that the sorbent temperature inside the reactor could be even higher, as we only measured the temperature after heat transfer through the wall. Furthermore, the IR camera identified the hottest point on the image. In this snapshot, the value is 77.6  $^\circ\text{C}$  (at the steel clamp attachment of the ground electrode), but since this point is variable over time, it was not included in the left graph. The steel clamp was only the hottest initially, due to Ohmic heating of the current flow and due to heat transfer from the reactor body. This is more visible in the steel clamp than in the aluminum ground electrode due to the low emissivity of aluminum. Later, the downstream area became warmer and the maximum temperature point shifted.

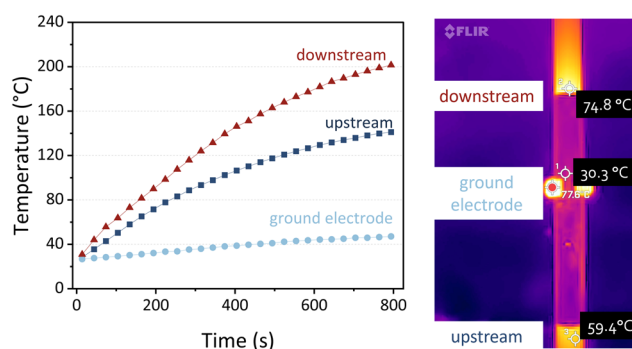


**Figure 5.** Temperature at the outside of the DBD reactor packed with zeolite 5A during plasma operation (left) and the thermal image (right), taken at 140 s. The grounded electrode remains dark in the image because the metal has a low emissivity (0.1–0.15) compared to the ceramic (0.95); hence, the IR camera cannot measure the temperature appropriately.

Both the upstream and downstream reactor walls heat up very quickly. Within 200 s, the temperature is higher than 60  $^\circ\text{C}$ , which can induce desorption according to the TPD (cf. Figure 4b). The temperature of the wall continuously increases up to 200  $^\circ\text{C}$ . During the cooldown period, the reactor wall temperature also remains above 80  $^\circ\text{C}$  within 400 s after switching off the plasma. This can explain the sustained desorption that we observed in Figure 4a and indicates that the temperature plays an important role in the desorption, although other mechanisms cannot be ruled out. Possibly, reactive plasma species, such as electrons, ions, radicals, and excited molecules produced in the plasma, can interact with the surface and also enhance the desorption, as discussed in the work by Yoshida et al.<sup>21</sup> where plasma desorption was much quicker than thermal desorption. However, these temperatures of DBD plasma are not enough for thermal  $\text{CO}_2$  splitting,<sup>18</sup> as demonstrated by the sudden drop in CO concentration in Figure 4a. The effect of plasma is twofold: (1) heating the material to induce desorption and (2) splitting the desorbed  $\text{CO}_2$  into CO. This combination is crucial to achieving real carbon utilization in the plasma–sorbent system.

**3.2.  $\text{CO}_2$  Adsorption Followed by Desorption in  $\text{Ar}/\text{CH}_4$  Plasma.** As discussed in the previous section, only  $\text{CO}_2$  adsorbs significantly, meaning that sorbent-based DRM is not feasible with a  $\text{CO}_2/\text{CH}_4$  mixture as the feed gas. Instead, an alternative approach can be implemented by introducing  $\text{CH}_4$  to the carrier gas during the desorption stage with plasma. To validate this,  $\text{CO}_2$ -saturated sorbents were flushed with a  $\text{CH}_4/\text{Ar}$  mixture and subsequently exposed to plasma in the same  $\text{CH}_4/\text{Ar}$  mixture. Detailed experimental procedures can be found in the SI, Sections S4 and S7. Figure 6 presents the concentrations as a function of time during the desorption step when the  $\text{Ar}/\text{CH}_4$  plasma is ignited.

The concentrations of  $\text{CO}_2$  and CO exhibit similar profiles as in the previous section, indicating that the  $\text{CH}_4/\text{Ar}$  plasma is also suitable to desorb  $\text{CO}_2$  and convert it to CO. The concentration of  $\text{CH}_4$  drops within the initial 200 s, due to three primary factors: (1)  $\text{CH}_4$  is consumed via nonoxidative coupling into higher hydrocarbons induced by the plasma, which also explains the drop observed in  $\text{CH}_4$  concentration in the blank experiments; (2) dilution of the relative concentration due to  $\text{CO}_2$  desorption from the sorbent into the gas phase; (3)  $\text{CH}_4$  consumption as a result of reactions with desorbed  $\text{CO}_2$ . Due to the latter two reasons, the  $\text{CH}_4$

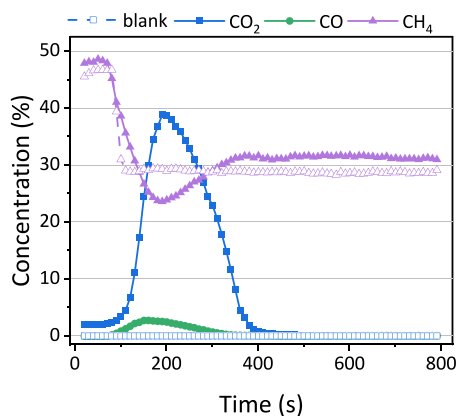


**Figure 6.** Concentration of CO<sub>2</sub>, CO, and CH<sub>4</sub> in the outlet stream during the desorption stage when the Ar/CH<sub>4</sub> plasma is ignited. The solid points are for the zeolite, while the open symbols are for the blank measurements with quartz.

concentration decreases to a lower level in the case of zeolite 5A compared to the blank experiment. Subsequently, it begins to increase and reaches a plateau, corresponding to the declining CO<sub>2</sub> desorption over time.

Interestingly, there is a small difference between the CH<sub>4</sub> concentrations of the blank and the zeolite after 500 s, even though the desorption is finished. The small deviation might be attributed to the water formation in the experiment with the zeolite sorbent, which can bind to the zeolite and influence the reaction, as discussed in more detail in Section 3.2.2. Indeed, even small amounts of H<sub>2</sub>O can influence the reaction,<sup>55</sup> which can explain this difference.

The estimated conversion based on the CO production is about  $7 \pm 1\%$ , with an estimated energy yield of  $0.0188 \text{ mmol kJ}^{-1}$ . This is significantly lower than the estimated conversion of  $15 \pm 1\%$  in Section 3.1.2 because other products such as water can be formed due to the CH<sub>4</sub> addition. Indeed, DRM should primarily occur during CO<sub>2</sub> desorption, i.e., between 100 and 400 s, and pure CH<sub>4</sub> conversion (i.e., nonoxidative coupling) takes place after 400 s. Although the measured spectra suggest the formation of C<sub>2</sub>H<sub>6</sub> and C<sub>2</sub>H<sub>2</sub> (SI, Section S8), quantification remains challenging due to their spectral overlap with CH<sub>4</sub> peaks. Therefore, we conducted additional GC measurements, supplementary to the FTIR measurement, for better analysis of products and reactions.

**3.2.1. Product Verification.** The results of the GC measurements are depicted in Figure 7. Due to limitations in the setup, we could only measure discrete points in time, as discussed in Section 2.1.

Not only H<sub>2</sub> is formed but also C<sub>2+</sub> hydrocarbons, including C<sub>2</sub>H<sub>6</sub>, C<sub>2</sub>H<sub>4</sub>, C<sub>2</sub>H<sub>2</sub>, and C<sub>3+</sub> products. Some CO<sub>2</sub> and CO are detected in the beginning at 100 and 200 s, similar to the desorption peak that we measured in Figure 6. For the blank material, there is no CO<sub>2</sub> and CO detected, corresponding to the fact that no adsorption of CO<sub>2</sub> occurred. As expected, the results with the sorbents are the same as the blank measurement after about 500 s. This is because the desorption of CO<sub>2</sub> is finished (Figure 6) and both materials display simply nonoxidative coupling of the CH<sub>4</sub> plasma. The results might be different if a catalyst would be included on the zeolite and could possibly alter the selectivity, which will be part of future work.

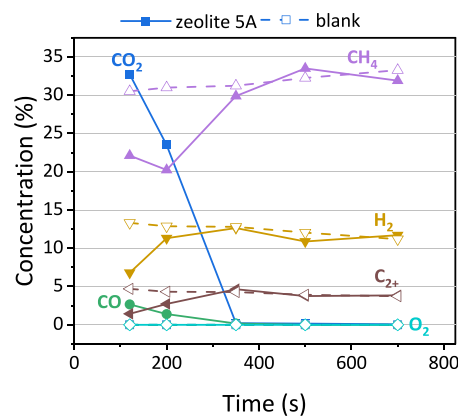


**Figure 7.** Concentration of all different components identified by GC for discrete points in time. The solid points are for the zeolite, while the open symbols are for the blank measurements with quartz.

From this figure, it is difficult to evaluate whether the desorbed CO<sub>2</sub> and CH<sub>4</sub> effectively interact during the possible DRM period (100–400 s). However, two observations do indicate the occurrence of DRM in our system. First, throughout the tests, no O<sub>2</sub> was detected, potentially due to the formation of H<sub>2</sub>O and CO, which consume O atoms generated in the plasma from CO<sub>2</sub>.<sup>56</sup> Second, condensation observed at the reactor outlet suggests the formation of liquid products, possibly including some oxygenated compounds, but primarily expected to be H<sub>2</sub>O, based on prior research in DBD plasma.<sup>57,58</sup> To further explore the role of H<sub>2</sub>O as an indicator for DRM, the relative humidity of the outlet gas stream was monitored with a humidity meter.

**3.2.2. The Role of H<sub>2</sub>O.** The results of the relative humidity in the outlet gas stream are shown in Figure 8. The measured H<sub>2</sub>O is an indicator for DRM; however, it is also important to understand the plasma–sorbent interaction. Note that the base humidity is not equal to zero, but since it remains consistent at about 25% after sufficiently flushing the system with dry input gas, the results of this experiment were deemed appropriate to understand different trends. The timing of 800 s was chosen to have an exact comparison to the desorption step in Figure 6.

First, we determined the humidity in the desorption procedure, where the time corresponds to the start of the desorption stage in which plasma is ignited and the desorption of CO<sub>2</sub> takes place. In Figure 8a, the humidity suddenly increases after 600 s for zeolite 5A. This indicates that the desorbed CO<sub>2</sub> is sufficient to react with CH<sub>4</sub> in the gas phase and confirms that the procedure in this work enables sorption-enhanced DRM, with H<sub>2</sub>O as a byproduct. For the blank measurement, this is not the case, since there is no desorbed CO<sub>2</sub> that could interact with CH<sub>4</sub> to form H<sub>2</sub>O, and the humidity stays constant. In addition to the desorption-based DRM, we also performed a typical “flow” experiment, where both CO<sub>2</sub> and CH<sub>4</sub> were simply used as feed gases during the plasma experiment in a 1/1 ratio and without any previous adsorption step, hence classical plasma-based DRM. The detailed results of this flow experiment are presented in the SI, Section S9. In Figure 8b, the humidity when using quartz sand packing rises rapidly, indicating that H<sub>2</sub>O is formed quickly in the blank experiments. For the zeolite 5A, however, there is a significant delay in the detection of H<sub>2</sub>O. Indeed, zeolite 5A is known to bind H<sub>2</sub>O very strongly thanks to its dipole.<sup>45</sup> Observations of the outlet confirm the results of the humidity

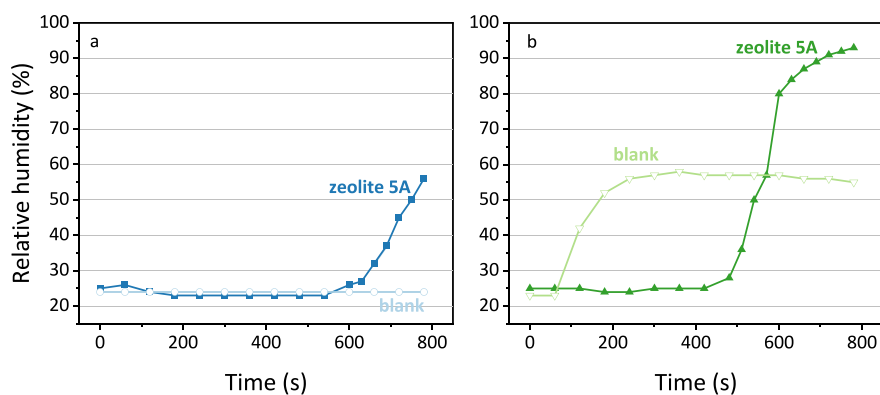


**Figure 8.** Relative humidity as a function of time for (a) the desorption procedure where the  $\text{CH}_4/\text{Ar}$  plasma is ignited on the zeolite with adsorbed  $\text{CO}_2$  from a previous step and (b) a typical flow plasma reaction with  $\text{CO}_2$  and  $\text{CH}_4$  as the feed gas without previous adsorption steps on the zeolite packing material.

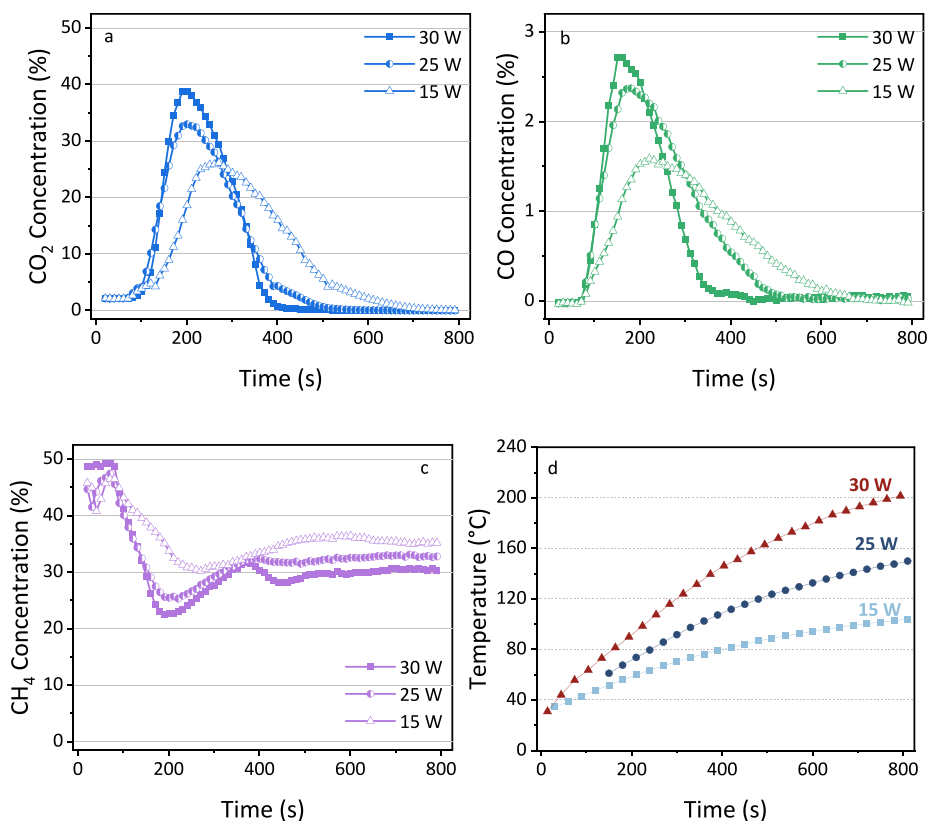


**Figure 9.** Concentration of  $\text{CO}_2$  (a), CO (b), and  $\text{CH}_4$  (c) as a function of time for different plasma powers. For clarity, there are no blank measurements displayed here. The downstream temperature of the reactor wall measured with a thermal camera is given in (d).

meter. When a higher humidity was measured, some condensation also formed in the outlet of the reactor, although there was not enough liquid for quantification.

This result could open the path to new applications in gas conversion with plasma technology. In DRM,  $\text{H}_2\text{O}$  is usually an unwanted byproduct in the outlet stream.<sup>59</sup> The zeolite material is able to capture the formed  $\text{H}_2\text{O}$  for *in situ* product removal, which can shift the equilibrium and enhance the conversion in plasma processes.<sup>60–62</sup> One could design a type of chemical looping process to exploit these properties, similar to catalysts.<sup>63</sup> For example, in the first stage, the DRM reaction can continue for about 450 s (or as long as  $\text{CO}_2$  desorption continues) with an  $\text{H}_2\text{O}$ -free product stream. In the second stage, before humidity increases, the feed gas can be switched

to a carrier gas (such as  $\text{N}_2$  and Ar) for a plasma treatment, to remove the  $\text{H}_2\text{O}$  and recover the sorbent material. Indeed, although most gas conversion research in typical flow plasma reactors aims for steady-state operation, these insights on shorter time scales provide a promising alternative.

**3.3. Influence of Power during Desorption.** To investigate the influence of discharge power, experiments were conducted using the same procedure at power levels of  $25.1 \pm 1$  W (ca. 25 W) and  $16.3 \pm 1.5$  W (ca. 15 W). The results are shown in Figure 9, alongside the previous results obtained from experiments conducted at 30 W. In all experiments, the same cooldown interval of 1800 s was maintained.



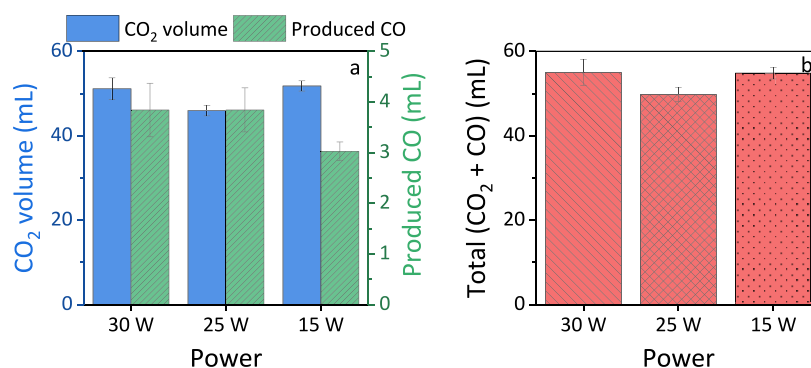


**Figure 10.** (a) Desorbed amount of CO<sub>2</sub> and measured CO and (b) the sum of CO<sub>2</sub> and CO for the three different powers tested in this work.

The concentration peaks of both CO<sub>2</sub> and CO shift to later times when lower power is applied, and we observe sharper peaks with a higher maximum in the case of ca. 30 W. These observations align with findings reported in a previous work.<sup>17</sup> The shift to later times (and a lower maximum) is attributed to fewer active species generated by the plasma and a more moderate heating effect at lower power, as indicated by the reactor wall temperature displayed in Figure 9d. Simultaneously, at lower plasma power, the measured concentration of CH<sub>4</sub> is higher. This results from the reduced CH<sub>4</sub> consumption at lower power.

Additionally, the total volumes of CO<sub>2</sub> and CO as well as the sum of both are shown in Figure 10. It can be observed that the overall sum of CO<sub>2</sub> and CO produced under different power settings is generally similar, with minor variations noted. There was no significant difference observed between the cases of 30 and 25 W. However, the production of CO was lower at 15 W. This discrepancy can be attributed to a combination effect of several factors. First, lower power led to slower desorption of CO<sub>2</sub> into the gas phase, affecting its conversion via gas-phase reactions (as shown in Figure 9). Additionally, plasma with lower power results in less energy input, meaning that fewer reactive species are generated to facilitate the conversion reaction. Compared to a reactor operating with constant reactant input (continuous feed gas flow of reactant), the plasma–sorbent system is inherently more complex. The observed combination effect cannot be adequately explained by one or two factors alone. Therefore, further in-depth investigation is necessary to fully understand the underlying mechanisms at play.

**3.4. Material Analysis.** As known in plasma catalysis and from previous work, exposure to plasma can change the physical properties of a packing material.<sup>17,54</sup> To investigate the effect of the different operating powers and the duration of the plasma treatment on the material, we measured the BET surface area and BHJ pore volume. The results are summarized in Table 2, and these values are in line with the range reported in the literature.<sup>64,65</sup>

The surface area and pore volume decrease when comparing the fresh sample to the treated samples. The carbon deposition from CH<sub>4</sub> plasma, which we could observe visually on the sample, plays a key role by clogging the porous structure. Pictures from the samples, as well as the results from a thermogravimetric analysis (TGA) are presented in the SI, Section S10.

The difference between the different powers is less significant. There is a minor increase in both the BET surface area and the BHJ pore volume when decreasing the power

**Table 2. Surface Area and Pore Volume of the Untreated Zeolite 5A Sorbent, Compared to the Different Procedures for Plasma Desorption<sup>a</sup>**

	BET surface area (m <sup>2</sup> ·g <sup>-1</sup> )	BHJ pore volume (cm <sup>3</sup> ·g <sup>-1</sup> )		BET surface area (m <sup>2</sup> ·g <sup>-1</sup> )	BHJ pore volume (cm <sup>3</sup> ·g <sup>-1</sup> )
untreated	577	0.242	untreated	577	0.242
30 W	<u>534</u>	<u>0.218</u>	1 run	544	0.224
25 W	536	0.219	<u>3 repeats</u>	<u>534</u>	<u>0.218</u>
15 W	546	0.224	<u>6 repeats</u>	523	0.212

<sup>a</sup>The benchmark of Section 3.2 is the desorption at ca. 30 W in 3 repeats, underlined in the table.

from ca. 30 W in the basic procedure to ca. 15 W. Furthermore, when we compare results for a single run, three repeats, and six consecutive repeats, they demonstrate a decrease in surface area and pore volume, which might inhibit long-term performance. Additional cleaning steps with for example O<sub>2</sub> plasma, might overcome this issue. Nevertheless, we observed no significant morphology change after six runs compared to the untreated sample, as indicated by the SEM images (Figure 11). Although some morphological changes might be too localized to capture with this SEM resolution, the parameters in Table 2 indicate that the overall effect will be very small.

#### 4. CONCLUSIONS AND OUTLOOK

In this work, a plasma–sorbent system for reactions of CO<sub>2</sub> and CH<sub>4</sub> was investigated. When using a CO<sub>2</sub>/CH<sub>4</sub> input mixture, zeolite 5A selectively absorbed CO<sub>2</sub> and acted as a filter to produce a purer CH<sub>4</sub> outlet stream. During the subsequent desorption step with Ar plasma, only CO<sub>2</sub> was desorbed from the material. We demonstrated the significant impact of plasma heating on the desorption process. During plasma operation, the reactor temperature could readily attain the levels necessary for thermal desorption of CO<sub>2</sub> from zeolite 5A. Furthermore, the production of CO arises from plasma-induced reactions and can be controlled instantly by switching the plasma on/off.

DRM from adsorbed components proved unfeasible via direct feeding of a CO<sub>2</sub>/CH<sub>4</sub> mixture since only CO<sub>2</sub> demonstrated significant adsorption and desorption. Instead, we explored an alternative approach, involving CH<sub>4</sub> addition during plasma-induced desorption of preadsorbed CO<sub>2</sub>. This yielded an output stream containing various value-added chemicals, including H<sub>2</sub>, CO, C<sub>2</sub>H<sub>6</sub>, C<sub>2</sub>H<sub>4</sub>, C<sub>2</sub>H<sub>2</sub>, and C<sub>3+</sub>. Although most of these products (except CO) could also be

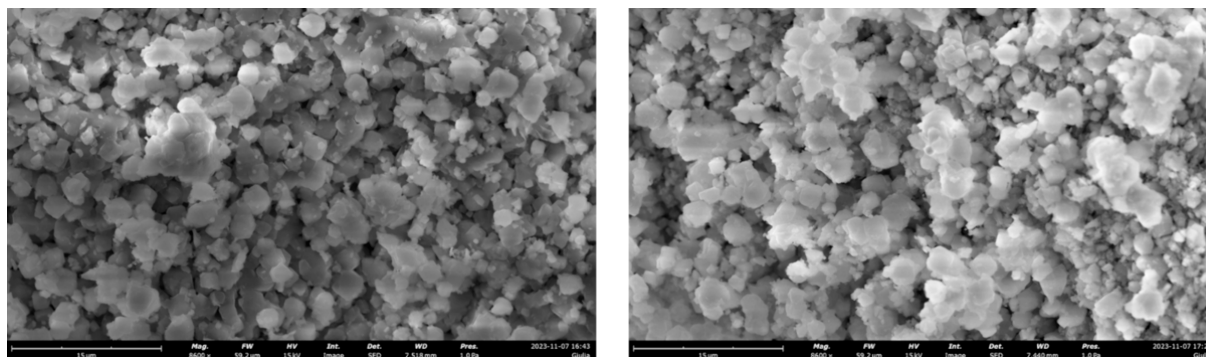


**Figure 11.** SEM images of the untreated zeolite (left) and the zeolite after six adsorption/desorption repeats (right).

formed by  $\text{CH}_4$  nonoxidative coupling only, the presence of  $\text{H}_2\text{O}$  suggested possible DRM reactions. Notably, zeolite 5A showed potential for *in situ* removal of  $\text{H}_2\text{O}$ , shifting the equilibrium and possibly enhancing the conversion in the plasma. Furthermore, the surface area and pore volume of zeolite 5A decreased after plasma exposure, caused by the carbon deposition on the sorbent. However, the material remained stable since we observed no significant morphological changes.

Overall, the plasma–sorbent system in this work provided an interesting proof of concept, but some remaining challenges require further investigation. The sorbent material could be tailored for a higher adsorption capacity and stability during gas conversion, as is already the subject in the field of material science for dual functional materials.<sup>66,67</sup> The possible competition between  $\text{CO}_2$  and  $\text{H}_2\text{O}$  adsorption could be further investigated. An ideal material for this process would be stable in the plasma discharge, resistant to carbon deposition, with a high adsorption capacity, and should adsorb both  $\text{CO}_2$  and  $\text{CH}_4$ . Alternatively, a mix of materials for either  $\text{CO}_2$  or  $\text{CH}_4$  adsorption could be more feasible. It should be noted that the field of  $\text{CH}_4$  adsorption remains challenging, especially in competition with  $\text{CO}_2$ , but some specifically tailored zeolites show promise.<sup>47,68</sup> Another modification would be to include a catalyst material on the sorbent, as studied in the field of plasma catalysis<sup>19</sup>; this could yield the production of different value-added chemicals. However, the influence on the adsorption–desorption mechanisms is an additional parameter to be considered.

Furthermore, the procedure for adsorption–flushing–desorption could be tuned for better performance, even at the lab scale. This includes optimization of the flow rate and time for each step. For instance, employing short or moderate flushing can retain weakly adsorbed  $\text{CO}_2$ , which can then be utilized in later stages. Moreover, in this study, Ar was used as the carrier gas for accurate measurement of transient concentrations, but this is not necessary for practical applications considering the additional cost. Exploring cost-effective carrier gases like  $\text{N}_2$  is needed, or even batch reactors can be considered, which can efficiently leverage plasma heating for desorption and offer longer reaction residence times. External heating could be investigated as well to speed up the desorption, although this would increase the energy cost and require careful tuning of the residence time to ensure sufficient conversion.

In addition, exploring innovation at the process level holds potential for a more practical utilization of mixed sources such as biogas. For instance, utilizing sorbents such as zeolite 5A,

which selectively adsorb  $\text{CO}_2$  as demonstrated in this study, allows for the initial separation of  $\text{CH}_4$  from the inlet stream during the adsorption step. Subsequently, this  $\text{CH}_4$  can be reintroduced into the reactor during desorption steps (via periodic operation with redirection of the flow or using a multireactor system) to conduct DRM with preadsorbed  $\text{CO}_2$ , as demonstrated in our paper. The  $\text{CO}_2/\text{CH}_4$  ratio can be tuned in this way, which will be beneficial, and the conversion can be enhanced due to the adsorption of produced  $\text{H}_2\text{O}$ , as also observed in our study.

Finally, the plasma reactor itself can also be investigated to enhance its performance. Both reactor design and operating parameters can significantly influence the conversion and energy efficiency, as investigated by many other studies in the field.<sup>69,70</sup> A multidisciplinary approach for all the above-mentioned areas is needed to investigate the promising potential of sorption-enhanced DRM.

## ■ ASSOCIATED CONTENT

### Supporting Information

The Supporting Information is available free of charge at <https://pubs.acs.org/doi/10.1021/acssuschemeng.4c02502>.

Contains the results from zeolite 4A test, as well as the adsorption capacity, Lissajous figures to describe the plasma power and specific experimental outline of each separate experiment; the pre-treatment results are presented, results from a TPD-MS test, additional figures on  $\text{CO}_2$  adsorption and  $\text{CH}_4$  flushing, detailed FTIR spectra, additional tests of the flow configuration and the results from the TGA (PDF)

## ■ AUTHOR INFORMATION

### Corresponding Author

**Sirui Li** – Research Group Inorganic Membranes and Membrane Reactors, Sustainable Process Engineering, Department of Chemical Engineering and Chemistry, Eindhoven University of Technology, Eindhoven S612 AP, The Netherlands; [orcid.org/0000-0002-2267-4335](https://orcid.org/0000-0002-2267-4335); Email: [s.li1@tue.nl](mailto:s.li1@tue.nl)

### Authors

**Rani Vertongen** – Research Group PLASMANT, Department of Chemistry, University of Antwerp, Antwerp 2610, Belgium  
**Giulia De Felice** – Research Group Inorganic Membranes and Membrane Reactors, Sustainable Process Engineering, Department of Chemical Engineering and Chemistry, Eindhoven University of Technology, Eindhoven S612 AP, The Netherlands

Huub van den Bogaard – Research Group Inorganic Membranes and Membrane Reactors, Sustainable Process Engineering, Department of Chemical Engineering and Chemistry, Eindhoven University of Technology, Eindhoven 5612 AP, The Netherlands

Fausto Gallucci – Research Group Inorganic Membranes and Membrane Reactors, Sustainable Process Engineering, Department of Chemical Engineering and Chemistry, Eindhoven University of Technology, Eindhoven 5612 AP, The Netherlands; [orcid.org/0000-0001-6379-773X](https://orcid.org/0000-0001-6379-773X)

Annemie Bogaerts – Research Group PLASMANT, Department of Chemistry, University of Antwerp, Antwerp 2610, Belgium; [orcid.org/0000-0001-9875-6460](https://orcid.org/0000-0001-9875-6460)

Complete contact information is available at:

<https://pubs.acs.org/10.1021/acssuschemeng.4c02502>

## Notes

The authors declare no competing financial interest.

## ACKNOWLEDGMENTS

We acknowledge financial support from the Fund for Scientific Research (FWO) Flanders (grant ID 110221N and grant ID V404823N) and the European Research Council (ERC) under the European Union's Horizon 2020 research and innovation program (grant agreement no. 810182 - SCOPE ERC Synergy project). We also thank Thijs van Raak for practical help with the experiments, and Pepijn Heirman and Robin De Meyer for the interesting discussions.

## REFERENCES

- (1) Masson-Delmotte, P.; Zhai, A.; Pirani, S. L.; Connors, C.; Péan, S.; Berger, N.; Caud, Y.; Chen, L.; Goldfarb, M. I.; Gomis, M.; Huang, K.; Leitzell, E.; Lonnoy, J. B. R.; Matthews, T. K.; Maycock, T.; Waterfield, O.; Yelekçi, R.; Yu, B.; Zhou, V.; Press, C. U. IPCC, 2021: Climate Change 2021: The Physical Science Basis. *Contribution of Working Group I to the Sixth Assessment Report of the Intergovernmental Panel on Climate Change*; 2021.
- (2) Mallapragada, D. S.; Dvorkin, Y.; Modestino, M. A.; Esposito, D. V.; Smith, W. A.; Hodge, B. M.; Harold, M. P.; Donnelly, V. M.; Nuz, A.; Bloomquist, C.; Baker, K.; Grabow, L. C.; Yan, Y.; Rajput, N. N.; Hartman, R. L.; Biddinger, E. J.; Aydil, E. S.; Taylor, A. D. Decarbonization of the Chemical Industry through Electrification: Barriers and Opportunities. *ChemRxiv. Cambridge: Cambridge Open Engage* **2023**, 7 (1), 23–41. 2022; *This content is a preprint and has not been peer-reviewed*
- (3) IEA Global Energy and Climate Model. <https://www.iea.org/reports/global-energy-and-climate-model> (accessed 2023–12–12).
- (4) Mac Dowell, N.; Fennell, P. S.; Shah, N.; Maitland, G. C. The Role of CO<sub>2</sub> Capture and Utilization in Mitigating Climate Change. *Nat. Clim Chang* **2017**, 7 (4), 243–249.
- (5) Abanades, J. C.; Rubin, E. S.; Mazzotti, M.; Herzog, H. J. On the Climate Change Mitigation Potential of CO<sub>2</sub> Conversion to Fuels. *Energy Environ. Sci.* **2017**, 10 (12), 2491–2499.
- (6) Perreault, P.; Kummamuru, N. B.; Gonzalez Quiroga, A.; Lenaerts, S. CO<sub>2</sub> Capture Initiatives: Are Governments, Society, Industry and the Financial Sector Ready? *Curr. Opin Chem. Eng.* **2022**, 38, No. 100874.
- (7) van der Spek, M.; Roussanaly, S.; Rubin, E. S. Best Practices and Recent Advances in CCS Cost Engineering and Economic Analysis. *International Journal of Greenhouse Gas Control* **2019**, 83, 91–104.
- (8) Seibel, B. A.; Walsh, P. J. Potential Impacts of CO<sub>2</sub> Injection on Deep-Sea Biota. *Science* **2001**, 294 (5541), 319–320. (1979)
- (9) Hepburn, C.; Adlen, E.; Beddington, J.; Carter, E. A.; Fuss, S.; Mac Dowell, N.; Minx, J. C.; Smith, P.; Williams, C. K. The

Technological and Economic Prospects for CO<sub>2</sub> Utilization and Removal. *Nature* **2019**, 575 (7781), 87–97.

(10) Breyer, C.; Khalili, S.; Bogdanov, D.; Ram, M.; Oyewo, A. S.; Aghahosseini, A.; Gulagi, A.; Solomon, A. A.; Keiner, D.; Lopez, G.; Ostergaard, P. A.; Lund, H.; Mathiesen, B. V.; Jacobson, M. Z.; Victoria, M.; Teske, S.; Pregger, T.; Fthenakis, V.; Rauegi, M.; Holttinen, H.; Bardi, U.; Hoekstra, A.; Sovacool, B. K. On the History and Future of 100% Renewable Energy Systems Research. *IEEE Access* **2022**, 10, 78176–78218.

(11) Hasan, M. M. F.; First, E. L.; Boukouvala, F.; Floudas, C. A. A Multi-Scale Framework for CO<sub>2</sub> Capture, Utilization, and Sequestration: CCUS and CCU. *Comput. Chem. Eng.* **2015**, 81, 2–21.

(12) Sun, S.; Sun, H.; Williams, P. T.; Wu, C. Recent Advances in Integrated CO<sub>2</sub> Capture and Utilization: A Review. *Sustain Energy Fuels* **2021**, 5 (18), 4546–4559.

(13) Erans, M.; Sanz-Pérez, E. S.; Hanak, D. P.; Clulow, Z.; Reiner, D. M.; Mutch, G. A. Direct Air Capture: Process Technology, Techno-Economic and Socio-Political Challenges. *Energy Environ. Sci.* **2022**, 15 (4), 1360–1405.

(14) Liu, G.; Sun, S.; Sun, H.; Zhang, Y.; Lv, J.; Wang, Y.; Zeng, J.; Yan, Z.; Wu, C. Integrated CO<sub>2</sub> Capture and Utilisation: A Promising Step Contributing to Carbon Neutrality. *Carbon Capture Science & Technology* **2023**, 7, No. 100116.

(15) Agliuzza, M.; Mezza, A.; Sacco, A. Solar-Driven Integrated Carbon Capture and Utilization: Coupling CO<sub>2</sub> Electroreduction toward CO with Capture or Photovoltaic Systems. *Appl. Energy* **2023**, 334, No. 120649.

(16) Xie, B.; Lovell, E.; Tan, T. H.; Jantarang, S.; Yu, M.; Scott, J.; Amal, R. Emerging Material Engineering Strategies for Amplifying Photothermal Heterogeneous CO<sub>2</sub> Catalysis. *Journal of Energy Chemistry* **2021**, 59, 108–125.

(17) Li, S.; Gallucci, F. CO<sub>2</sub> Capture and Activation with a Plasma-Sorbent System. *Chemical Engineering Journal* **2022**, 430, 132979.

(18) Snoeckx, R.; Bogaerts, A. Plasma Technology - a Novel Solution for CO<sub>2</sub> Conversion? *Chem. Soc. Rev.* **2017**, 46 (19), 5805–5863.

(19) Bogaerts, A.; Neyts, E. C.; Guitella, O.; Murphy, A. B. Foundations of Plasma Catalysis for Environmental Applications. *Plasma Sources Sci. Technol.* **2022**, 31 (5), 53002.

(20) Slaets, J.; Aghaei, M.; Ceulemans, S.; Van Alphen, S.; Bogaerts, A. CO<sub>2</sub> and CH<sub>4</sub> Conversion in “Real” Gas Mixtures in a Gliding Arc Plasmatron: How Do N<sub>2</sub> and O<sub>2</sub> Affect the Performance? *Green Chem.* **2020**, 22 (4), 1366–1377.

(21) Yoshida, K.; Okubo, M.; Yamamoto, T. Distinction between nonthermal Plasma and Thermal Desorptions for NO<sub>x</sub> and CO<sub>2</sub>. *Appl. Phys. Lett.* **2007**, 90 (13), No. 131501.

(22) Li, S.; Ongis, M.; Manzolini, G.; Gallucci, F. Non-Thermal Plasma-Assisted Capture and Conversion of CO<sub>2</sub>. *Chemical Engineering Journal* **2021**, 410, No. 128335.

(23) Kaikkonen, T. *Dual-Functional Materials for Combined CO<sub>2</sub> Capture and Non-Thermal Plasma-Assisted Conversion*; Tampere University: Tampere, 2023. <https://trepo.tuni.fi/bitstream/handle/10024/144819/KaikkonenTero.pdf?sequence=2> (accessed 2023–07–27).

(24) Gorky, F.; Nambo, A.; Carreon, M. L. Cold Plasma-Metal Organic Framework (MOF)-177 Breathable System for Atmospheric Remediation. *Journal of CO<sub>2</sub> Utilization* **2021**, 51, No. 101642.

(25) Gorky, F.; Nguyen, H. M.; Krishnan, K.; Lucero, J. M.; Carreon, M. L.; Carreon, M. A. Plasma-Induced Desorption of Methane and Carbon Dioxide over Silico Aluminophosphate Zeolites. *ACS Appl. Energy Mater.* **2023**, 6 (8), 4380–4389.

(26) Moss, M.; Reed, D. G.; Allen, R. W. K.; Styring, P. Integrated CO<sub>2</sub> Capture and Utilization Using Non-Thermal Plasmas. *Front Energy Res.* **2017**, 5, 20.

(27) Chen, G.; Buck, F.; Kistner, I.; Widenmeyer, M.; Schiestel, T.; Schulz, A.; Walker, M.; Weidenkaff, A. A Novel Plasma-Assisted Hollow Fiber Membrane Concept for Efficiently Separating Oxygen from CO in a CO<sub>2</sub> Plasma. *Chemical Engineering Journal* **2020**, 392, 123699.

- (28) Okubo, M.; Takahashi, K.; Kamiya, S.; Kuroki, T. High-Efficiency Carbon Dioxide Reduction Using nonthermal Plasma Desorption. *IEEE Trans Ind. Appl.* **2018**, *54* (6), 6422–6429.
- (29) Yamasaki, H.; Kamei, S.; Kuroki, T.; Okubo, M. Adsorbed CO<sub>2</sub> Dissociation Using Argon and Helium nonthermal Plasma Flows. *IEEE Trans Ind. Appl.* **2020**, *56* (6), 6983–6989.
- (30) Wakimoto, H.; Yamasaki, H.; Kuroki, T.; Okubo, M. High-Efficiency Carbon Dioxide Reduction Using Catalytic nonthermal Plasma Desorption. *Mech. Eng. J.* **2023**, *10* (2), 22–00191.
- (31) Grande, C. A. Biogas Upgrading by Pressure Swing Adsorption. In *Biofuel's Engineering Process Technology*; Bernardes, M. A.; dos, S., Ed.; IntechOpen: Rijeka, 2011; p Ch. 3.
- (32) EPA. *Basic Information about Landfill Gas*. <https://www.epa.gov/lmop/basic-information-about-landfill-gas> (accessed 2023–11–15).
- (33) Peeters, F.; Butterworth, T. Electrical Diagnostics of Dielectric Barrier Discharges. In *Atmospheric Pressure Plasma*; Anton, N.; Zhiqiang, C., Eds.; IntechOpen: Rijeka, 2018; p Ch. 2.
- (34) Bencloski, J. W. Air Temperature and Relative Humidity: A Simulation. *Journal of Geography* **1982**, *81* (2), 64–65.
- (35) Merel, J.; Clause, M.; Meunier, F. Experimental Investigation on CO<sub>2</sub> Post-Combustion Capture by Indirect Thermal Swing Adsorption Using 13X and 5A Zeolites. *Ind. Eng. Chem. Res.* **2008**, *47* (1), 209–215.
- (36) Collins, F.; Rozhkovskaya, A.; Outram, J. G.; Millar, G. J. A Critical Review of Waste Resources, Synthesis, and Applications for Zeolite LTA. *Microporous Mesoporous Mater.* **2020**, *291*, No. 109667.
- (37) Shi, X.; Xiao, H.; Azarabadi, H.; Song, J.; Wu, X.; Chen, X.; Lackner, K. S. Sorbents for the Direct Capture of CO<sub>2</sub> from Ambient Air. *Angew. Chem., Int. Ed.* **2020**, *59* (18), 6984–7006.
- (38) Ray, B.; Churipard, S. R.; Peter, S. C. An Overview of the Materials and Methodologies for CO<sub>2</sub> Capture under Humid Conditions. *J. Mater. Chem. A Mater.* **2021**, *9* (47), 26498–26527.
- (39) Younas, M.; Sohail, M.; Leong, L. K.; Bashir, M. J.; Sumathi, S. Feasibility of CO<sub>2</sub> Adsorption by Solid Adsorbents: A Review on Low-Temperature Systems. *International Journal of Environmental Science and Technology* **2016**, *13* (7), 1839–1860.
- (40) Wanten, B.; Vertongen, R.; De Meyer, R.; Bogaerts, A. Plasma-Based CO<sub>2</sub> Conversion: How to Correctly Analyze the Performance? *Journal of Energy Chemistry* **2023**, *86*, 180–196.
- (41) Navascués, P.; Cotrino, J.; González-Elipse, A. R.; Gómez-Ramírez, A. Plasma Assisted CO<sub>2</sub> Dissociation in Pure and Gas Mixture Streams with a Ferroelectric Packed-Bed Reactor in Ambient Conditions. *Chemical Engineering Journal* **2022**, *430*, 133066.
- (42) Mofarahi, M.; Ghohipour, F. Gas Adsorption Separation of CO<sub>2</sub>/CH<sub>4</sub> System Using Zeolite 5A. *Microporous Mesoporous Mater.* **2014**, *200*, 1–10.
- (43) Al-Naddaf, Q.; Rownaghi, A. A.; Rezaei, F. Multicomponent Adsorptive Separation of CO<sub>2</sub>, CO, CH<sub>4</sub>, N<sub>2</sub>, and H<sub>2</sub> over Core-Shell Zeolite-5A@MOF-74 Composite Adsorbents. *Chemical Engineering Journal* **2020**, *384*, No. 123251.
- (44) Qi, K.; Gao, L.; Li, X.; He, F. Research Progress in Gas Separation and Purification Based on Zeolitic Materials. *Catalysts* **2023**, *13* (5), 855.
- (45) Poling, B. E.; Prausnitz, J. M.; O'Connell, J. P. *Properties of Gases and Liquids*; McGraw-Hill, 2004.
- (46) Jackson, R. B.; Abernethy, S.; Canadell, J. G.; Cargnello, M.; Davis, S. J.; Féron, S.; Fuss, S.; Heyer, A. J.; Hong, C.; Jones, C. D.; Damon Matthews, H.; O'Connor, F. M.; Pisciotta, M.; Rhoda, H. M.; de Richter, R.; Solomon, E. I.; Wilcox, J. L.; Zickfeld, K. Atmospheric Methane Removal: A Research Agenda. *Philosophical Transactions of the Royal Society A: Mathematical, Physical and Engineering Sciences* **2021**, *379* (2210), No. 20200454.
- (47) Wang, Q.; Yu, Y.; Li, Y.; Min, X.; Zhang, J.; Sun, T. Methane Separation and Capture from Nitrogen Rich Gases by Selective Adsorption in Microporous Materials: A Review. *Sep Purif Technol.* **2022**, *283*, No. 120206.
- (48) Wang, J.; Fu, R.; Wen, S.; Ning, P.; Helal, M. H.; Salem, M. A.; Xu, B. B.; El-Bahy, Z. M.; Huang, M.; Guo, Z.; Huang, L.; Wang, Q. Progress and Current Challenges for CO<sub>2</sub> Capture Materials from Ambient Air. *Adv. Compos. Hybrid Mater.* **2022**, *5* (4), 2721–2759.
- (49) Ozkan, A.; Dufour, T.; Silva, T.; Britun, N.; Snyders, R.; Bogaerts, A.; Reniers, F. The Influence of Power and Frequency on the Filamentary Behavior of a Flowing DBD—Application to the Splitting of CO<sub>2</sub>. *Plasma Sources Sci. Technol.* **2016**, *25* (2), No. 025013.
- (50) Ramakers, M.; Michielsen, I.; Aerts, R.; Meynen, V.; Bogaerts, A. Effect of Argon or Helium on the CO<sub>2</sub> Conversion in a Dielectric Barrier Discharge. *Plasma Processes and Polymers* **2015**, *12* (8), 755–763.
- (51) Wang, T.; Liu, H.; Xiong, X.; Feng, X. Conversion of Carbon Dioxide to Carbon Monoxide by Pulse Dielectric Barrier Discharge Plasma. *IOP Conf. Ser.: Earth Environ. Sci.* **2017**, *52* (1), 12100.
- (52) Vertongen, R.; Bogaerts, A. How Important Is Reactor Design for CO<sub>2</sub> Conversion in Warm Plasmas? *Journal of CO<sub>2</sub> Utilization* **2023**, *72*, No. 102510.
- (53) Brehmer, F.; Welzel, S.; Klarenaar, B. L. M.; van der Meiden, H. J.; van de Sanden, M. C. M.; Engeln, R. Gas Temperature in Transient CO<sub>2</sub> Plasma Measured by Raman Scattering. *J. Phys. D Appl. Phys.* **2015**, *48* (15), No. 155201.
- (54) Neyts, E. C.; Ostrikov, K. K.; Sunkara, M. K.; Bogaerts, A. Plasma Catalysis: Synergistic Effects at the Nanoscale. *Chem. Rev.* **2015**, *115* (24), 13408–13446.
- (55) Kolb, T.; Kroker, T.; Voigt, J. H.; Gericke, K.-H. Wet Conversion of Methane and Carbon Dioxide in a DBD Reactor. *Plasma Chemistry and Plasma Processing* **2012**, *32* (6), 1139–1155.
- (56) Navascués, P.; Cotrino, J.; González-Elipse, A. R.; Gómez-Ramírez, A. Plasma Assisted Dry Reforming of Methane: Syngas and Hydrocarbons Formation Mechanisms. *Fuel Process. Technol.* **2023**, *248*, No. 107827.
- (57) Li, S.; Sun, J.; Gorbanev, Y.; van't Veer, K.; Loenders, B.; Yi, Y.; Kenis, T.; Chen, Q.; Bogaerts, A. Plasma-Assisted Dry Reforming of CH<sub>4</sub>: How Small Amounts of O<sub>2</sub> Addition Can Drastically Enhance the Oxygenate Production—Experiments and Insights from Plasma Chemical Kinetics Modeling. *ACS Sustain Chem. Eng.* **2023**, *11* (42), 15373–15384.
- (58) Slaets, J.; Loenders, B.; Bogaerts, A. Plasma-Based Dry Reforming of CH<sub>4</sub>: Plasma Effects vs. Thermal Conversion. *Fuel* **2024**, *360*, No. 130650.
- (59) Snoeckx, R.; Wang, W.; Zhang, X.; Cha, M. S.; Bogaerts, A. Plasma-Based Multi-Reforming for Gas-To-Liquid: Tuning the Plasma Chemistry towards Methanol. *Sci. Rep.* **2018**, *8* (1), 15929.
- (60) Rouwenhorst, K. H. R.; Lefferts, L. Plasma-based Conversions with in Situ Product Removal. *Plasma Processes Polym.* **2023**, *21* (1), No. e2200244.
- (61) Vertongen, R.; Trenchev, G.; Van Loenhout, R.; Bogaerts, A. Enhancing CO<sub>2</sub> Conversion with Plasma Reactors in Series and O<sub>2</sub> Removal. *Journal of CO<sub>2</sub> Utilization* **2022**, *66*, No. 102252.
- (62) Rouwenhorst, K. H. R.; Mani, S.; Lefferts, L. Improving the Energy Yield of Plasma-Based Ammonia Synthesis with In Situ Adsorption. *ACS Sustain Chem. Eng.* **2022**, *10* (6), 1994–2000.
- (63) Delikonstantis, E.; Scapinello, M.; Singh, V.; Poelman, H.; Montesano, C.; Martini, L. M.; Tosi, P.; Marin, G. B.; Van Geem, K. M.; Galvita, V. V.; Stefanidis, G. D. Exceeding Equilibrium CO<sub>2</sub> Conversion by Plasma-Assisted Chemical Looping. *ACS Energy Lett.* **2022**, *7* (6), 1896–1902.
- (64) Mendes, P. A. P.; Ribeiro, A. M.; Gleichmann, K.; Ferreira, A. F. P.; Rodrigues, A. E. Separation of CO<sub>2</sub> /N<sub>2</sub> on Binderless 5A Zeolite. *Journal of CO<sub>2</sub> Utilization* **2017**, *20*, 224–233.
- (65) Khoramzadeh, E.; Mofarahi, M.; Lee, C.-H. Equilibrium Adsorption Study of CO<sub>2</sub> and N<sub>2</sub> on Synthesized Zeolites 13X, 4A, 5A, and Beta. *J. Chem. Eng. Data* **2019**, *64* (12), 5648–5664.
- (66) Omodolor, I. S.; Otor, H. O.; Andonegui, J. A.; Allen, B. J.; Alba-Rubio, A. C. Dual-Function Materials for CO<sub>2</sub> Capture and Conversion: A Review. *Ind. Eng. Chem. Res.* **2020**, *59* (40), 17612–17631.
- (67) Chen, J.; Xu, Y.; Liao, P.; Wang, H.; Zhou, H. Recent Progress in Integrated CO<sub>2</sub> Capture and Conversion Process Using Dual

Function Materials: A State-of-the-Art Review. *Carbon Capture Science & Technology* **2022**, *4*, No. 100052.

(68) Kim, J.; Maiti, A.; Lin, L.-C.; Stolaroff, J. K.; Smit, B.; Aines, R. D. New Materials for Methane Capture from Dilute and Medium-Concentration Sources. *Nat. Commun.* **2013**, *4* (1), 1694.

(69) Zhang, S.; Gao, Y.; Sun, H.; Fan, Z.; Shao, T. Dry Reforming of Methane by Microsecond Pulsed Dielectric Barrier Discharge Plasma: Optimizing the Reactor Structures. *High Voltage* **2022**, *7* (4), 718–729.

(70) Wang, X.; Gao, Y.; Zhang, S.; Sun, H.; Li, J.; Shao, T. Nanosecond Pulsed Plasma Assisted Dry Reforming of CH<sub>4</sub>: The Effect of Plasma Operating Parameters. *Appl. Energy* **2019**, *243*, 132–144.

## Supporting Information

# Sorption-enhanced dry reforming of methane in a DBD plasma reactor for single-stage carbon capture and utilization

Rani Vertongen<sup>1</sup>, Giulia De Felice,<sup>2</sup> Huub van den Bogaard,<sup>2</sup> Fausto Gallucci,<sup>2</sup>  
Annemie Bogaerts<sup>1</sup> and Sirui Li<sup>2\*</sup>

<sup>1</sup> Research group PLASMANT, Department of Chemistry, University of Antwerp,  
Universiteitsplein 1, 2610 Antwerp, Belgium.

<sup>2</sup> Research group Inorganic Membranes and Membrane Reactors, Sustainable Process Engineering, Department  
of Chemical Engineering and Chemistry, Eindhoven University of Technology,  
De Rondom 70, Eindhoven 5612 AP, the Netherlands.

\*Corresponding author: dr. Sirui Li, email: s.li1@tue.nl

Number of pages: 11

Number of figures: 11

Number of tables: 2

## S1. Zeolite 4A

Although a detailed material study was out of scope for this work, we performed some pretests with zeolite 4A. As the results in Figure SI - 1 demonstrate, zeolite 4A has a much lower adsorption capacity, with an early breakthrough curve and small CO<sub>2</sub> volume during desorption. This is in line with previous investigations on adsorbents.<sup>1</sup> The material has a large effect on the performance and leaves room for improvement in future work.

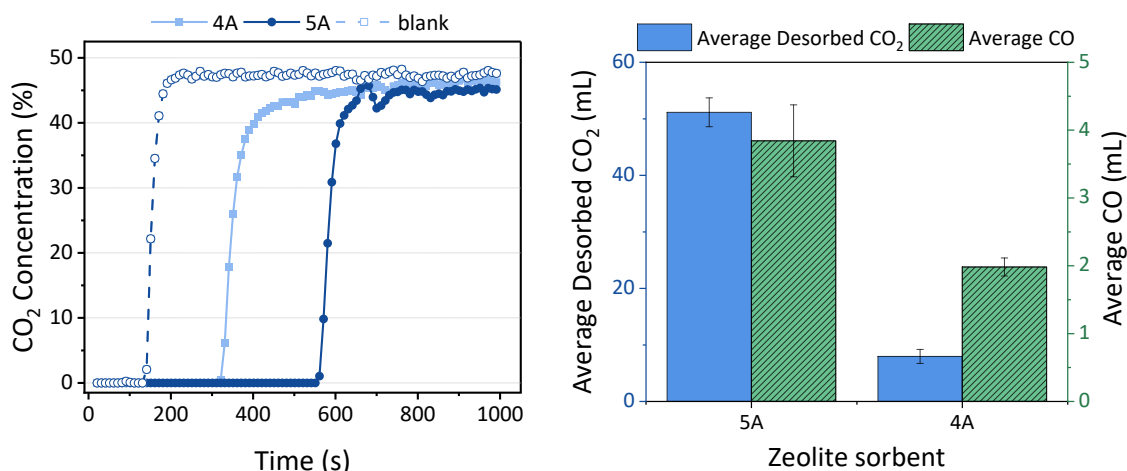


Figure SI - 1 Comparison of zeolite 4A and 5A in terms of (left) CO<sub>2</sub> adsorption as a function of time for a single experiment and (right) CO<sub>2</sub> desorption and CO production averaged over three repeated experiments; note the different scales for CO<sub>2</sub> and CO. The solid points are for the zeolite, while the open symbols are for the blank measurements with quartz.

## S2. Adsorption capacity

We repeated each experiment three times on the same powder. To check the viability of this approach, we plot the adsorbed amount of CO<sub>2</sub> for each separate run in Figure SI - 2. These results are obtained with the procedure from Section 3.2 in the main paper, to study the influence of the CH<sub>4</sub> plasma during desorption. The adsorbed volume of CO<sub>2</sub> is slightly higher in the first run compared to the second and third runs (1% decrease), possibly due to carbon deposition (see Section 3.4 in the main paper) or H<sub>2</sub>O adsorption (see Section 3.2.2 in the main paper), but the error on the average remains very small. In other words, this approach is suitable for a quantitative comparison between the procedures.

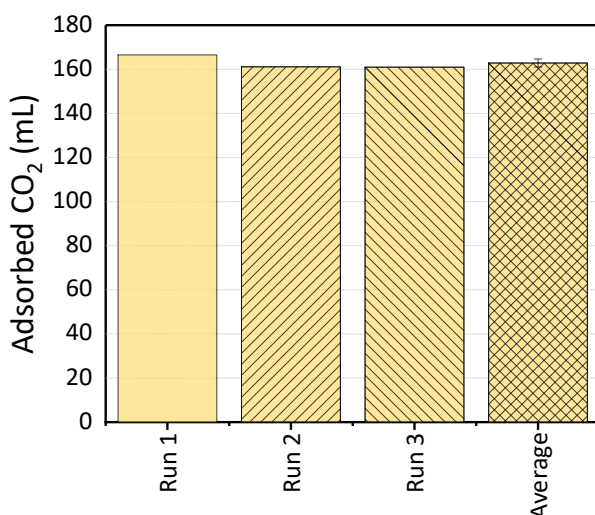


Figure SI - 2 Adsorbed amount of CO<sub>2</sub> for three runs separately and summarized by the average.

### S3. Plasma power

A typical Lissajous figure to calculate the power is presented in Figure SI - 3. The plasma power is nearly constant in most experiments, the measured plasma power is on average  $31 \pm 1.5$  W. To simplify the notation, we describe this as “ca. 30 W” in the main paper.

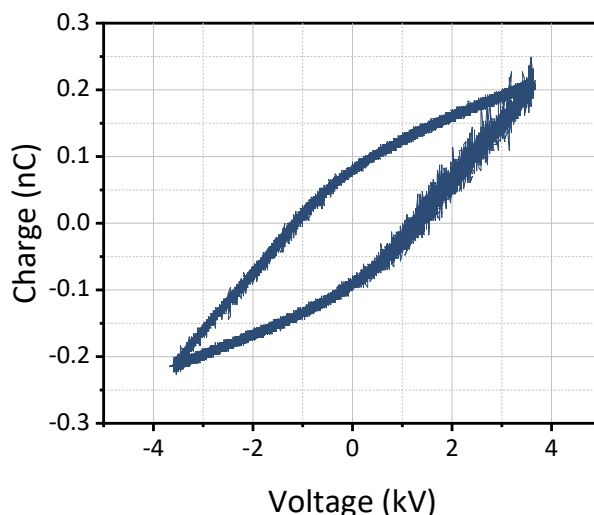


Figure SI - 3 Q-V diagram, also called Lissajous plot,<sup>2</sup> to illustrate the power calculation during plasma-desorption (zeolite 5A packing, 20/20 mL<sub>n</sub>/min CH<sub>4</sub>/Ar, CO<sub>2</sub> desorption).

### S4. Specific experimental outline

The exact outline of each experiment is presented in this Section.

Table SI - 1 Overview of the adsorption-desorption procedure with a mixed CO<sub>2</sub>/CH<sub>4</sub> flow during the adsorption stage, as presented in the main paper in Section 3.1.

	Time (s)	Ar (mL <sub>n</sub> /min)	CO <sub>2</sub> (mL <sub>n</sub> /min)	CH <sub>4</sub> (mL <sub>n</sub> /min)	Plasma power (W)
<b>Adsorption</b>	800	20	20	20	0
<b>Flushing</b>	1000	100	0	0	0
<b>Desorption</b>	800	40	0	0	30

Table SI - 2 Overview of the adsorption-desorption procedure with CH<sub>4</sub> addition in the desorption step, as presented in the main paper in Section 3.2.

	Time (s)	Ar (mL <sub>n</sub> /min)	CO <sub>2</sub> (mL <sub>n</sub> /min)	CH <sub>4</sub> (mL <sub>n</sub> /min)	Plasma power (W)
<b>Adsorption</b>	800	20	20	0	0
<b>Flushing</b>	1000	50	0	50	0
<b>Desorption</b>	800	20	0	20	30



## S5. Pre-treatment results

We performed the pre-treatment of zeolite 5A utilizing an Ar plasma for 1800 s at a plasma power of ca. 30 W. A typical result is presented in Figure SI - 4. The initial drop in CO<sub>2</sub> concentration is due to the flushing of the lines. At about 100 s, there is a clear desorption peak of CO<sub>2</sub> that was previously adsorbed from the ambient atmosphere and full desorption is achieved at 500s. The small CO peak is the result of CO<sub>2</sub> conversion. Preliminary tests showed that additional drying of the sample for 24h gave the same results as applying the plasma-treatment only.

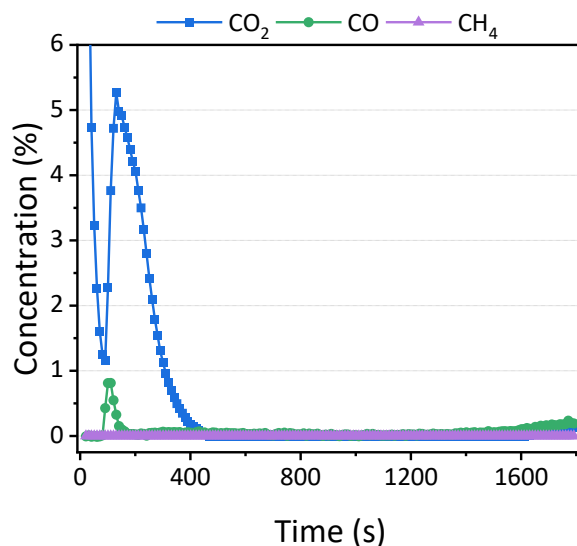


Figure SI - 4 Concentration of CO<sub>2</sub> and CH<sub>4</sub> in the outlet stream during pretreatment.

The concentrations during the cool down phase fall quickly below 0.2%, hence, we do not present these results in a graph.

## S6. Approximate comparison with TPD-MS

A direct comparison between the plasma experiment and a thermal test is not possible. The plasma-induced heating is rather complex, since the reactor is heated not through a contact surface inside/outside of the reactor, but by the microdischarges and chemical reactions in the plasma, causing hot spots and a non-uniform heating profile. Still, we made an approximate comparison between the plasma test and a TPD-MS measurement. The procedure was performed according to the specifications in Table 1 in the main paper, but after the flushing stage, the sample was transferred to a sample holder for TPD-MS. A heating rate of 15°C/min was applied for the first 500 s, and then 8°C/min for the time of 500-800 s, to mimic the temperatures in Figure 5. The results are presented in Figure SI - 5.

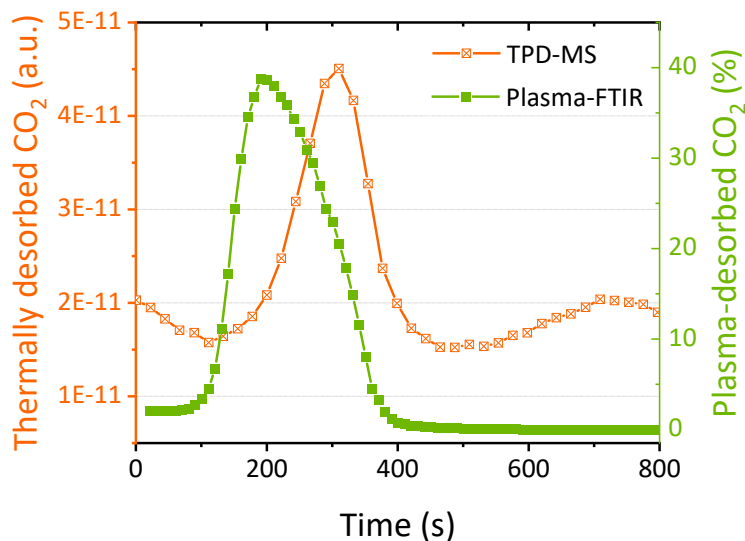


Figure SI - 5 CO<sub>2</sub> concentration measured in an approximate TPD-MS test (left axis) and through the usual plasma-FTIR experiment (right axis). Note that the scales of this figure are not representative, since the MS signal is in arbitrary units.

There is a sharp peak of desorption around 300 s, but the peak in the plasma test is earlier. Since the temperature setting of TPD-MS was chosen based on the temperature measurement of the surface of the plasma reactor (Figure 5 in the main paper), this applied temperature is lower than the actual temperature of the bed, which can explain the late appearance of the peak. Importantly, no CO was measured in the TPD-MS test, confirming that no CO<sub>2</sub> conversion occurs at these temperatures without the plasma.

## S7.CO<sub>2</sub> adsorption and CH<sub>4</sub> flushing

Similar to Section 3.1.1 in the main paper for the CO<sub>2</sub>/CH<sub>4</sub> mixture, we measured the concentrations during CO<sub>2</sub> adsorption and CH<sub>4</sub> flushing as a function of time with an in-line FTIR, and the results are presented in Figure SI - 6.

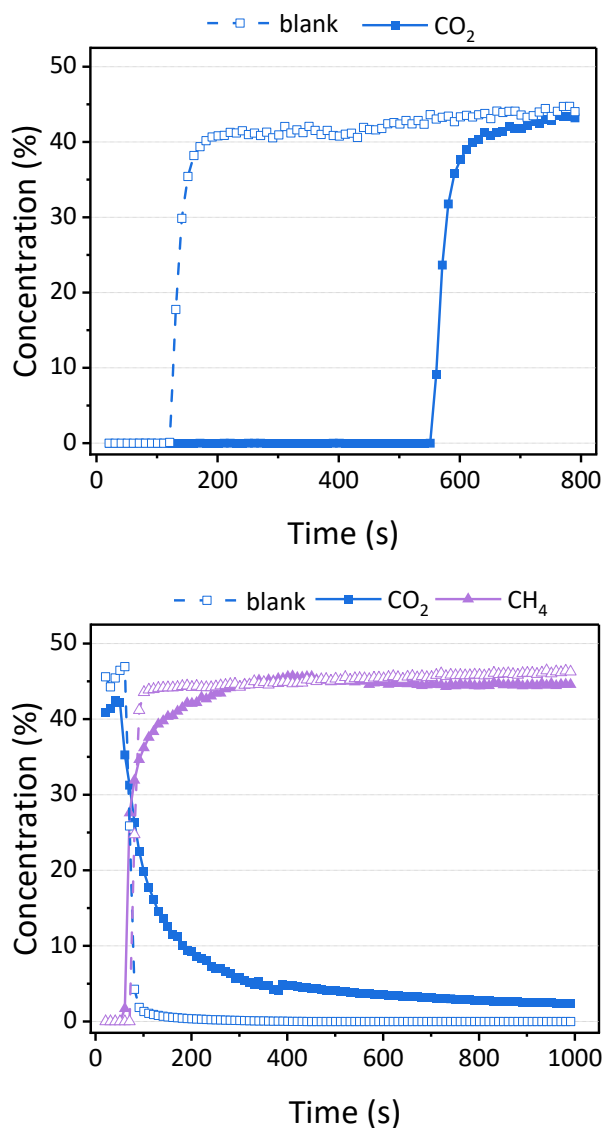


Figure SI - 6 Concentration of CO<sub>2</sub> and CH<sub>4</sub> in the outlet stream during the adsorption (top) and flushing (bottom) stage. The solid points are for the zeolite, while the open symbols are for the blank measurements with quartz.

The adsorption of CO<sub>2</sub> has a breakthrough around 500-600 s, even when no CH<sub>4</sub> is present in the mixture, hence very similar to the experiments in Section 3.1.1 for the CO<sub>2</sub>/CH<sub>4</sub> mixture. This is expected because the same flow rate of CO<sub>2</sub> is maintained in both cases due to the lower limit of the mass flow controllers. The CO<sub>2</sub> concentration remains slightly lower than the blank, although it continues to increase slowly after the breakthrough point. This might be related to slow, continued adsorption, but initial tests revealed that this amount is not significant for these experiments.

CH<sub>4</sub> is added during the flushing step to saturate the volume between the pores and eliminate any possible delays on the mass flow controllers during the desorption phase. It has a similar profile over the zeolite as over the quartz material.

Despite the varying composition of the gas during the plasma desorption process, the plasma power remains constant, as shown in Figure SI - 7. The measured plasma power is on average  $31.6 \pm 0.1$  W. The fact that the plasma power remains constant can be expected since the ionization potentials of  $\text{CO}_2$  and  $\text{CH}_4$  are similar.<sup>3</sup>

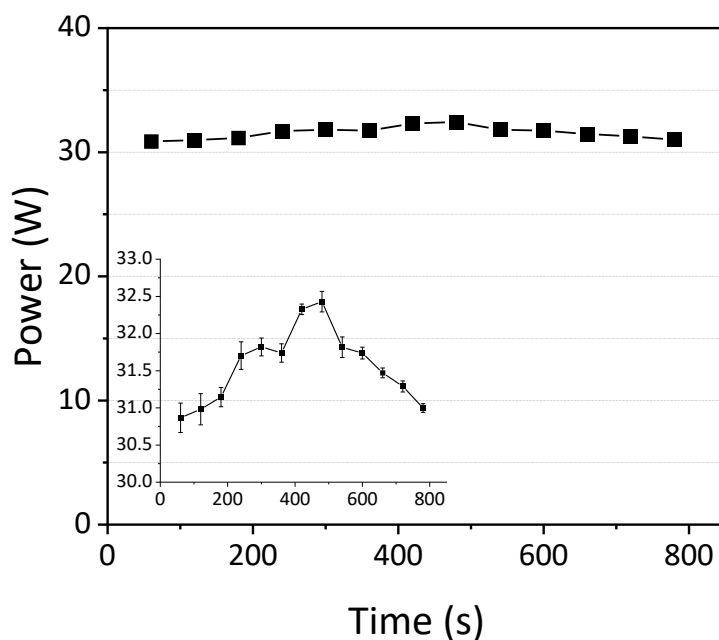


Figure SI - 7 Plasma power as a function of time during the desorption step. The error bars are too small to be visible. The inset presents a finer resolution on the y-axis.

## S8. FTIR spectra

A typical FTIR spectrum of an experiment of Section 3.2 in the main paper is presented in Figure SI - 8. The peaks were designated based on the NIST database.<sup>3</sup> At 300 s, there is clear  $\text{CO}_2$  desorption and some conversion to  $\text{CO}$ , but the desorption seems over by 400 s. At both points in time, the production of  $\text{C}_2\text{H}_6$  is observed, as well as  $\text{C}_2\text{H}_2$ , an indication of methane non-oxidative coupling.<sup>4</sup>

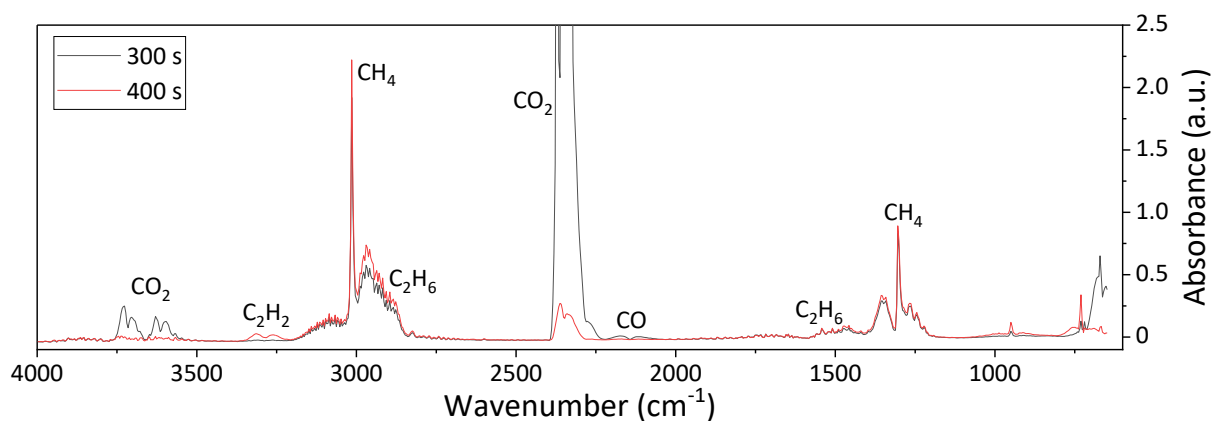


Figure SI - 8 FTIR spectrum of the  $\text{CH}_4$  plasma-induced desorption of pre-adsorbed  $\text{CO}_2$ . Note that the y-axis is presented on a smaller scale to visualize the smaller peaks. In the full resolution, no peaks are saturated in the spectrum.

## S9. Sorption vs flow configuration

In order to compare the desorption procedure with the typical “flow” plasma reaction, we performed two experiments with a CH<sub>4</sub> and CO<sub>2</sub>/CH<sub>4</sub> flow at a plasma power of ca. 30 W without an adsorption step.

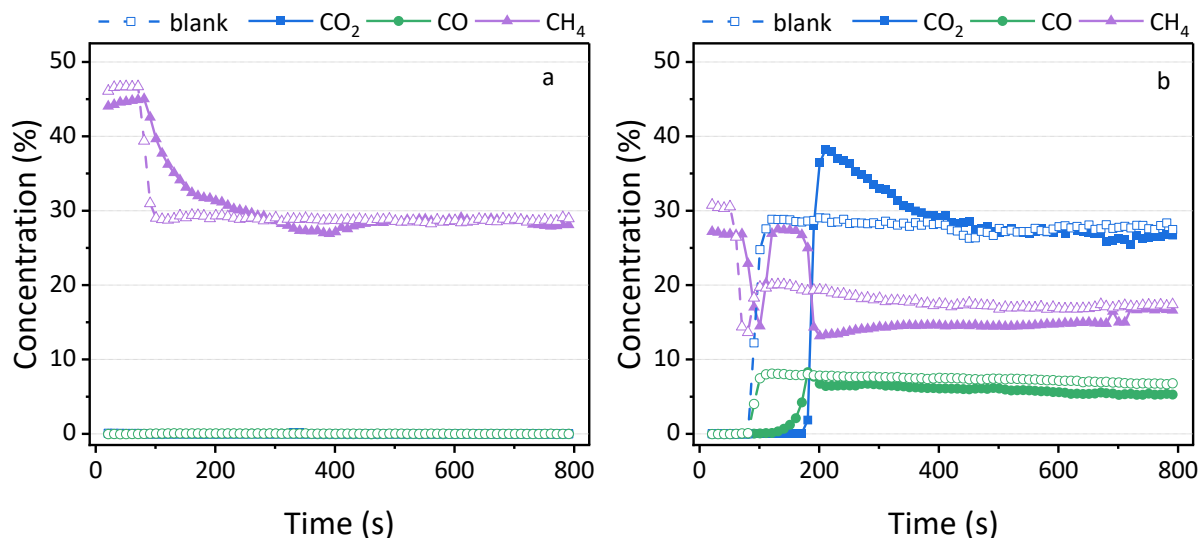


Figure SI - 9 Concentration of CO<sub>2</sub>, CO and CH<sub>4</sub> in the outlet stream during a typical flow plasma in (a) CH<sub>4</sub> and (b) CO<sub>2</sub>/CH<sub>4</sub>. The solid points are for the zeolite, while the open symbols are for the blank measurements with quartz.

Figure SI - 9a presents the pure CH<sub>4</sub> plasma. There is a slight delay in the drop of the CH<sub>4</sub> concentration, due to the length of the lines. There is no CO<sub>2</sub> or CO measured, as expected. The CH<sub>4</sub> concentration drops quicker in the blank (quartz sand) measurement than in the zeolite. Perhaps some adsorption-desorption effects still play a role for CH<sub>4</sub>, since there is no CO<sub>2</sub> to compete with the binding sites on the zeolite. After 500 s, they both reach the same equilibrium concentration. Since no CO<sub>2</sub> is present, no H<sub>2</sub>O is formed, and the results are not included in Section 3.2.2 in the main paper.

In Figure SI - 9b, a typical DRM plasma is presented, for which the results from the humidity meter are displayed in the main paper in Section 3.2.2. To prevent any adsorption of CO<sub>2</sub>, a quick switching of gases is needed. First, Ar/CH<sub>4</sub> is inserted at 40/20 mL<sub>n</sub>/min to flush. Then, the plasma is ignited and the flow is quickly switched to Ar/CH<sub>4</sub>/CO<sub>2</sub> 20/20/20 mL<sub>n</sub>/min. There is a slight delay (< 30 s) in the CO<sub>2</sub> concentration in the blank experiment (quartz sand) due to the later addition. Interestingly, the delay is even larger in zeolite 5A, followed by a higher desorption peak around 200s. This suggests that there is still some CO<sub>2</sub> adsorbed on the material, followed by immediate desorption, before reaching the equilibrium concentration. At equilibrium after 600s, it seems that the CH<sub>4</sub> conversion is higher (i.e. lower CH<sub>4</sub> concentration) than the CO<sub>2</sub> conversion, typical for DRM reactions with a CO<sub>2</sub>/CH<sub>4</sub> feed.

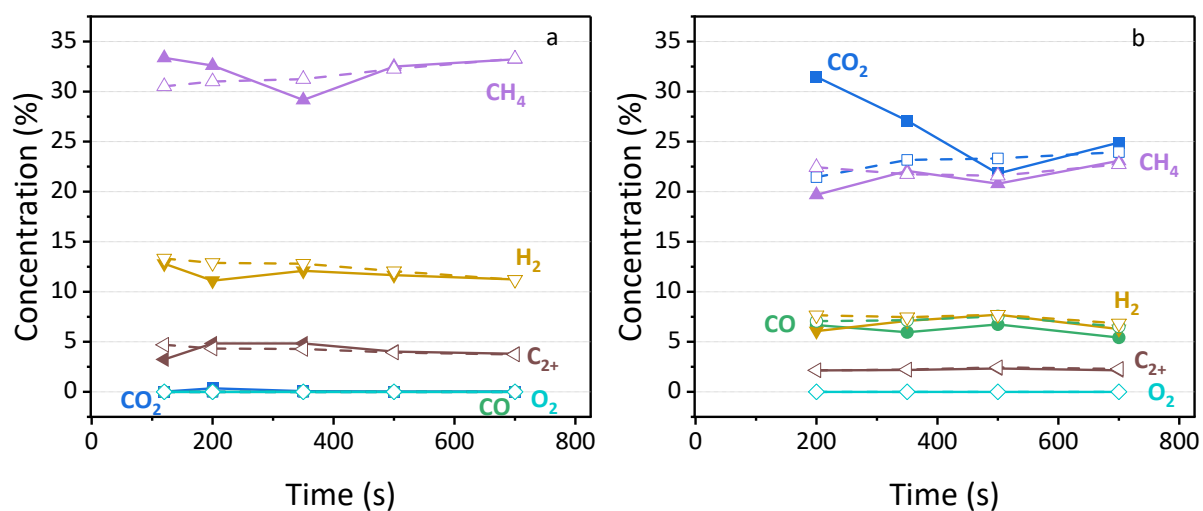


Figure SI - 10 Volume fraction of all different components identified by GC for discrete points in time in (a) a CH<sub>4</sub> plasma and (b) a CO<sub>2</sub>/CH<sub>4</sub> plasma. The solid points are for the zeolite, while the open symbols are for the blank measurements with quartz.

The results of the GC are also in line with expectations from a typical flow plasma reactor. The CH<sub>4</sub> plasma shows significant H<sub>2</sub> and hydrocarbon production. For the CO<sub>2</sub>/CH<sub>4</sub> mixture, the concentration of CO<sub>2</sub> is higher at first, in line with the small desorption peak that was observed in the FTIR results around 210 s, but then all concentrations reach the same equilibrium as in the blank measurement.

## S10. TGA results

The thermogravimetric analysis was conducted with approximately 50 mg of material, in an air atmosphere at atmospheric pressure and a rise of 5°C/min. The results are shown in Figure SI - 11.

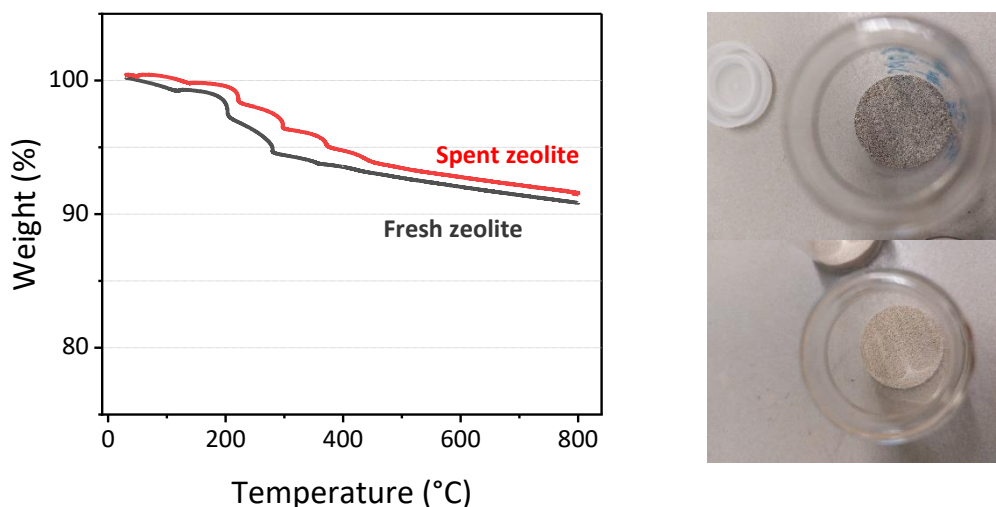


Figure SI - 11 Weight as a function of the programmed temperature in the TGA for the fresh zeolite sample and the zeolite sample after the reaction as described in the main paper. Pictures of the spent (top) and fresh (bottom) samples are included.

Visually, there is a clear difference between the fresh sample and the spent zeolite. The spent zeolite is darker in color, probably due to the carbon deposition. In the TGA, the initial profiles are very similar for the fresh and the spent material. Volatiles and CO<sub>2</sub> adsorbed from ambient air can play a role, as well as H<sub>2</sub>O desorption which is known to contribute (in the range up to 400°C<sup>5</sup>). In the curve of the spent sample, there are two subtle peaks in the range of 300-450 °C, but the overall carbon deposition seems limited compared to the literature on TGA of zeolites with coke.<sup>6,7</sup>

The fresh zeolite demonstrates slightly more weight decrease than the spent sample, for which two explanations are possible. First, the fresh zeolite might contain strongly adsorbed water that is removed during the TGA procedure, while in the spent sample, the plasma previously removed the H<sub>2</sub>O. Second, the carbon on the spent sample might block the pores so that less ambient CO<sub>2</sub> and H<sub>2</sub>O could adsorb in the time between the plasma treatment and TGA. Indeed, after the plasma procedure, all CO<sub>2</sub> and H<sub>2</sub>O should be desorbed from the material, and some carbon deposition is formed. However, the DBD reactor then must be opened to retrieve the material and perform the TGA in a different machine. Hence, the spent sample is open to the ambient atmosphere, but it has a slightly lower available surface for adsorption of ambient molecules compared to the fresh sample due to the carbon deposition.

## References

- (1) Wilson, S. M. W.; Kennedy, D. A.; Tezel, F. H. Adsorbent Screening for CO<sub>2</sub>/CO Separation for Applications in Syngas Production. *Sep Purif Technol* **2020**, *236*, 116268. <https://doi.org/10.1016/j.seppur.2019.116268>.
- (2) Peeters, F.; Butterworth, T. Electrical Diagnostics of Dielectric Barrier Discharges. In *Atmospheric Pressure Plasma*; Anton, N., Zhiqiang, C., Eds.; IntechOpen: Rijeka, 2018; p Ch. 2. <https://doi.org/10.5772/intechopen.80433>.
- (3) *NIST Standard Reference Database Number 69*. <https://doi.org/10.18434/T4D303>.
- (4) Lee, D. H.; Song, Y.-H.; Kim, K.-T.; Lee, J.-O. Comparative Study of Methane Activation Process by Different Plasma Sources. *Plasma Chemistry and Plasma Processing* **2013**, *33* (4), 647–661. <https://doi.org/10.1007/s11090-013-9456-6>.
- (5) Gómez, L.; Martínez, I.; Navarro, M. V.; García, T.; Murillo, R. Sorption-Enhanced CO and CO<sub>2</sub> Methanation (SEM) for the Production of High Purity Methane. *Chemical Engineering Journal* **2022**, *440*, 135842. <https://doi.org/10.1016/j.cej.2022.135842>.
- (6) Ochoa, A.; Ibarra, Á.; Bilbao, J.; Arandes, J. M.; Castaño, P. Assessment of Thermogravimetric Methods for Calculating Coke Combustion-Regeneration Kinetics of Deactivated Catalyst. *Chem Eng Sci* **2017**, *171*, 459–470. <https://doi.org/10.1016/j.ces.2017.05.039>.
- (7) Ortega, J. M.; Gayubo, A. G.; Aguayo, A. T.; Benito, P. L.; Bilbao, J. Role of Coke Characteristics in the Regeneration of a Catalyst for the MTG Process. *Ind Eng Chem Res* **1997**, *36* (1), 60–66. <https://doi.org/10.1021/ie9507336>.